Max-Planck-Institut
für Meteorologie

REPORT No. 36

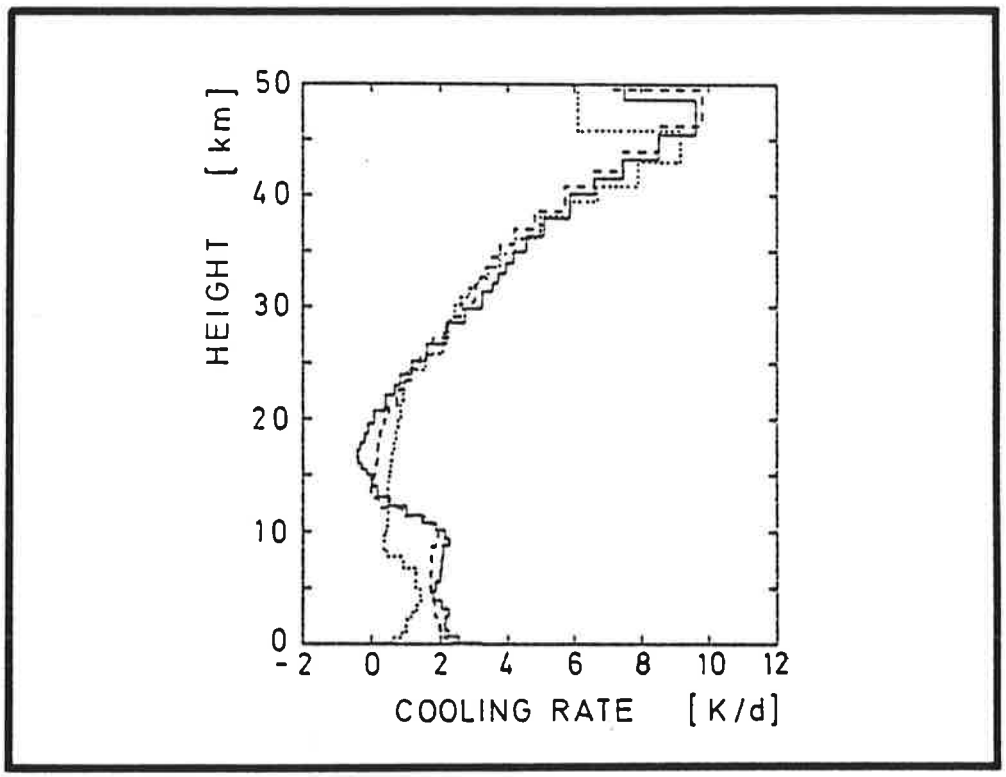

LINE-BY-LINE MODEL FOR THE CALCULATION OF INFRARED RADIATION FLUXES AND COOLING RATES IN CLEAR SKY ATMOSPHERES

by

HEINZ-DIETER HOLLWEG

HAMBURG, JULY 1989

AUTHOR:

HEINZ-DIETER HOLLWEG

MAX-PLANCK-INSTITUT
FUER METEOROLOGIE

COVER: Clear sky atmospheric cooling rates in the infrared for the tropical (solid curve), the midlatitude summer (dashed), and the subarctic winter (pointed) model atmospheres of McClatchey et al. (1978).

MAX-PLANCK-INSTITUT
FUER METEOROLOGIE
BUNDESSTRASSE 55
D-2000 HAMBURG 13
F.R. GERMANY

Tel.: (040) 4 11 73-0
Telex: 211092
Telemail: MPI.Meteorology
Telefax: (040) 4 11 73-298

REPb36

Line-by-Line Model for the Calculation of Infrared Radiation Fluxes and Cooling Rates in Clear Sky Atmospheres

H.-D. Hollweg
Max-Planck-Institut für Meteorologie
Hamburg

Abstract

A line-by-line model for the purpose of proving the influence of the absorption line parameters and the performance of the spectral resolution on evaluating radiative transfer has been developed for clear sky conditions in the infrared. It has been found that for small spectral ranges a resolution scheme with grouping subintervals according to the distribution of lines in conjunction with numerical Gaussian quadrature of different orders which depend on the absorption line ranges, assures high accuracy. For larger spectral intervals a resolution scheme using constant subintervals with 0.01 cm^{-1} widths in conjunction with an eight point Gaussian quadrature gives sufficient accuracy.

The influence of overlapping of absorption bands has been examined and it has been found that for the demands of models using fast approximative algorithms only overlapping of simultaneously two bands in the IR has to be considered. However, the inclusion of the 14 μm ozone band to the corresponding overlapping bands of H_2O and CO_2 improves the accuracy in the lower stratosphere considerably. The weak CO_2 band at 10.4 μm should be additionally included to the 9.6 μm ozone band and the water vapor continuum range, if drastically enlarged carbon dioxide concentration are considered.

Finally, the influence of the uncertainties of line parameter values on radiation transfer has been considered. For the assumption of an error of $\pm$ 10 % for all line strenghts and halfwidths an error margin of up to 10 % for the cooling rates in the stratosphere and a maximum about 4 % in the troposphere has been found.

1
Introduction

Climate investigations are only thinkable with the inclusion of radiation processes. The most straightforward application of radiation theory is done by line-by-line models and as this designation already indicates: each absorption line of each absorber has to be considered in conjunction with radiative sources and scattering processes.

Of course, this treatment would require too much computation time in climate models, so various parameterizations of radiation transfer have been developed (see e.g. the review article of Stephens [1984]). Nevertheless, because of the lack of measurments, line-by-line models serve as benchmarks for the approximative radiative properties.

However, even for this purpose one is obliged to apply approximations in order to keep calculation times reasonable. For instance, one strategy is to seperate the calculation of radiative properties into: firstly, evaluating transmissions line-by-line at various suitably chosen pressure and temperature values, and secondly, interpolating fluxes and cooling rates for any atmospheric profiles from the tabulated transmissions. This has been done for example by Fels and Schwarzkopf (1981) using a modified version of the line-by-line code of Drayson (1966); by Scott and Chedin (1981) using the code of Scott (1974); and by Chou and Kouvaris (1986) using precomputed transmissions by Chesters and Arking (1985).

This proceeding is advantageous if one is interested in radiative transfer calculations for a variety of atmospheric profiles without changing line parameters on which the calculation of transmission functions are based. However, the line-by-line model presented in this paper is intended as a benchmark and a tool for the development of approximate radiative transfer codes. From this, more concern has been put in testing the influence of various absorption coefficient formulations and approximations, than to supply fluxes for a set of atmospheric conditions. Therefore, the direct calculation of the transmission functions for various pressure–temperature levels within the atmosphere is prefered.

The following points list the processes in evaluating radiative properties which require most of the calculation time:

- the spectral resolution,
- the calculation of the absorption coefficients,
- the integration with respect to height,
- and the integration over the zenith angle.

The spectrum may be resolved by steps with constant widths (Chou and Arking; 1980) or by subintervals with nonconstant widths distributed according to the line centres (Kunde and Maguire; 1974). And the integration with respect to these subintervals may be carried out with different numerical quadratures.

The determination of the absorption coefficients is the most intricate problem. Here, we are faced with many physical properties, e.g. the distribution of lines and bands and, more substantially, with uncertainties in the absorption coefficients for many reasons. In order to save computation time most line-by-line models use the application of cutting off absorption lines in a certain distance from the centres. Another way of reducing computation time by approximating the absorption coefficients is that by Scott (1974). He shifts absorption lines to take advantage of a

mathematical simplification he proposes.

The treatment of the integration with respect to height in order to receive high accuracy depends on the subdivision of the given atmosphere into layers. If the layers are thin enough to assure almost homogeneity, then the calculated absorption coefficients can be considered as to be constant within each layer. If not, then numerical integration schemes have to be applied, or at least an assumption of the lapse rate of the absorption coefficients between the boundaries of each layer is necessary.

Finally, the integration with respect to the zenith angle is performed most accurately by numerical quadrature. Simplifications may be obtained by applying the diffusivity factor of 1.66 or by tabulated functions of the optical thickness (Liu and Schmetz, 1988). However, the numerical integration over the zenith angle requires only negligible computation time compared to the above mentioned processes.

In the present paper results of a line-by-line model for calculating radiation flux densities and cooling rates in a clear sky plane-parallel atmosphere in the infrared (IR) are reported. At first the integration of the radiative transfer equation for a plane-parallel layer is performed in section 2, followed by the integration of the optical thickness in section 3, where assumptions concerning the lapse rate of nonconstant concentrations are proposed which allow the analytical integration of the optical thickness. After providing the equations for the absorption coefficients of central ranges and wings of lines, numerical approximations used for economical reasons are discussed. In section 4 the spectral resolution is examined in view of numerical quadrature, and the widths and distribution of the subintervals. In section 5 calculated fluxes are compared with results of line-by-line models recorded in the ICRCCM study (WMO 1984). Next the influence of overlapping of absorption bands is discussed. Finally, estimates of errors in the absorption line parameters on the calculation of fluxes and atmospheric cooling rates are presented.

2
Equation of Radiative Transfer

We start with the equation of radiative transfer for plane-parallel layers which can be found in standard text books (e.g. Liou, 1980).

$$\mu \frac{dL_\nu(\tau_\nu, \mu, \phi)}{d\tau_\nu} = L_\nu(\tau_\nu, \mu, \phi) - J_\nu(\tau_\nu, \mu, \phi) \tag{1}$$

Here L_ν denotes the spectral radiance, J_ν the source function, τ_ν the optical thickness (for definition see section 3), μ the cosine of the zenith angle, and ϕ the azimuth angle. For convenience the index indicating the dependence on the wavenumber ν will be omitted in the following.

First we consider a plane-parellel atmosphere divided into layers with the upper boundary denoted by the subscript 2 the lower with 1. The geometry of such a layer is shown in Fig. 1 .

Fig. 1:

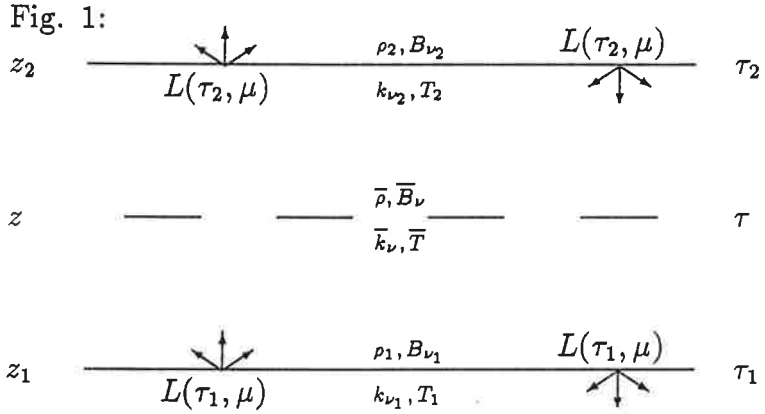

What we want to know are the upward and downward radiances at the boundaries of each layer for a clear nonscattering atmosphere in local thermal equilibrium in the IR. With the seperation in up- and downward components we get equations (2) and (3) with B denoting the Planck function depending on temperature T.

$$L^\uparrow(\tau_2, \mu) = L^\uparrow(\tau_1, \mu) e^{-(\tau_1 - \tau_2)/\mu} + \int_{\tau_2}^{\tau_1} B(T) e^{-(\tau' - \tau_2)/\mu} \frac{d\tau'}{\mu} \tag{2}$$

$$L^\downarrow(\tau_1, \mu) = L^\downarrow(\tau_2, \mu) e^{-(\tau_1 - \tau_2)/\mu} + \int_{\tau_2}^{\tau_1} B(T) e^{-(\tau_1 - \tau')/\mu} \frac{d\tau'}{\mu} \tag{3}$$

A general solution of the integrals are not known, but with the assumption of the Planck function being linearized (Zdunkowski et al.,1974)

$$B(\tau) := B_0 + B^*\tau \tag{4}$$

$$B^* = \frac{B_2 - B_1}{\tau_2 - \tau_1} \qquad \text{and} \qquad B_0 = \frac{B_1\tau_2 - B_2\tau_1}{\tau_2 - \tau_1}$$

an analytical integration is possible and equations (5) and (6) are received.

$$\begin{aligned} L^{\uparrow}(\tau_2,\mu) &= L^{\uparrow}(\tau_1,\mu)e^{-(\tau_1-\tau_2)/\mu} \\ &\quad + (B_0 + B^*\mu)(1 - e^{-(\tau_1-\tau_2)/\mu}) + B^*(\tau_2 - \tau_1 e^{-(\tau_1-\tau_2)/\mu}) \end{aligned} \tag{5}$$

$$\begin{aligned} L^{\downarrow}(\tau_1,\mu) &= L^{\downarrow}(\tau_2,\mu)e^{-(\tau_1-\tau_2)/\mu} \\ &\quad + (B_0 - B^*\mu)(1 - e^{-(\tau_1-\tau_2)/\mu}) + B^*(\tau_1 - \tau_2 e^{-(\tau_1-\tau_2)/\mu}) \end{aligned} \tag{6}$$

Integrating the radiances wih respect to the zenith and azimuth angles with the assumption of horizontal homogeneity supplies the spectral flux density F_ν. The further integration from wavenumber ν_1 to ν_2 yields the total flux density $F_{\Delta\nu}$ within the given wavenumber interval $\Delta\nu$.

$$F^{\uparrow\downarrow}_{\Delta\nu}(\tau) = \int_{\nu_1}^{\nu_2} F^{\uparrow\downarrow}_{\nu}\, d\nu = \int_{\nu_1}^{\nu_2}\int_0^{2\pi}\int_0^1 L^{\uparrow\downarrow}_{\nu}(\tau,\mu,\phi)\mu\, d\mu\, d\phi\, d\nu \tag{7}$$

Because Eq. (7) cannot be integrated analytically numerical Gaussian quadrature is applied for both, the integrations with respect to μ and ν. The letters N and O denote the numbers of Gaussian weights g and points relative to μ and ν within the subinterval $\Delta\nu_j$. The summation (the letter M) of the subintervals yields the total interval $\Delta\nu$. The order of quadrature may be varied within each subinterval.

$$F^{\uparrow\downarrow}_{\Delta\nu}(\tau) \approx \sum_{j=1}^{M}\sum_{k=1}^{N}\sum_{l=1}^{O} g_{kj}\, g_{lj}\, L^{\uparrow\downarrow}_{\nu_{klj}}(\tau,\mu_{kj})\mu_{kj}\Delta\nu_j \tag{8}$$

Finally the cooling rate in a layer is given by

$$\frac{\partial T}{\partial t} = \frac{g}{c_p} div_p \vec{F}_{\Delta\nu}\ . \tag{9}$$

Approximated cooling rates for layers are calculated from the differences of the net flux densities at the layer boundaries.

3
Determination of the Optical Thickness

For calculating fluxes and cooling rates it is necessary to provide a formulation of the interaction of radiation with the material of the layer throughout its path. In our case of a clear nonscattering atmosphere the normal optical thickness simplifies to the form given in Eq. (10) with the absorption coefficient k_{ν_i} of the i-th gaseous component, the height z, the absorber density ρ_i, the absorber concentration q_i, and the gravitational acceleration g.

$$d\tau_{\nu_i} = -k_{\nu_i}\rho_i dz = k_{\nu_i}\frac{q_i}{g}\,dp \tag{10}$$

To evaluate the optical thickness we have to:

- design a model atmosphere,
- consider the calculation of the absorption coefficients,
- and integrate Eq. (10).

The total normal optical thickness will then be the sum of all components.

3.1
Atmospheric Profiles

Of course, a model designed for calculating radiation transfer has to be applicable to any atmospheric condition which mays happen to occur. Usually, the atmospheric profiles are provided in the form of specifications of temperature, pressure, and density or concentration at discrete heights. Because of the atmosphere divided into layers at fixed pressure levels for the purpose of computing cooling rates, the atmospheric properties have to be interpolated to these levels and, if possible, to be expressed as functions of pressure within the layers.

The fixing of the pressure levels has been proved by Morcrette and Fouquart (1985) in detail in changing the number of layers. They conclude that an atmospheric model should include about twenty well suited layers in the stratosphere and about the same number in the troposphere, too.

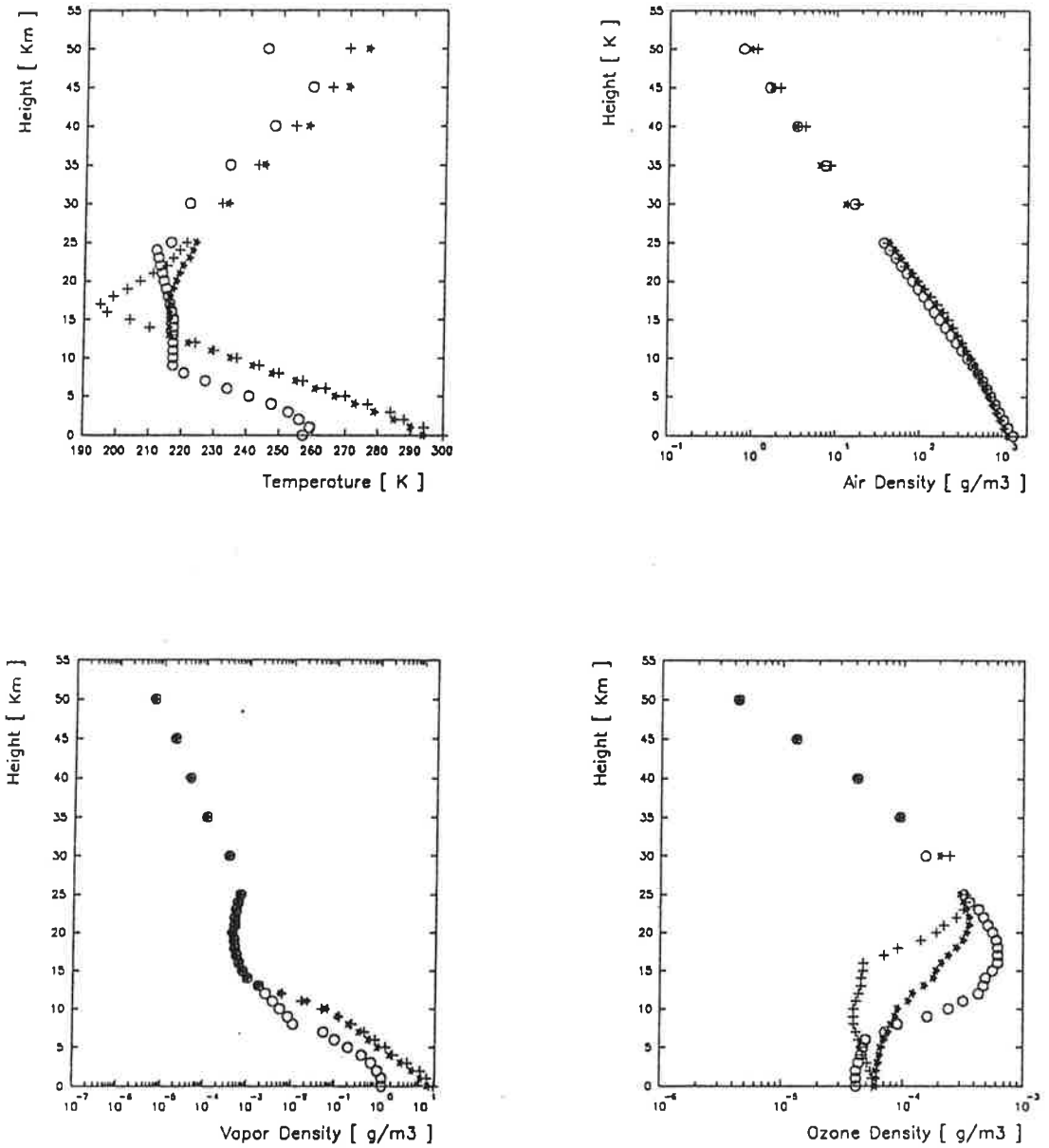

Fig. 2: Atmospheric profiles given by McClatchey et al. (1978) for the tropics (crosses), the midlatitude summer (asterisks) and the subarctic winter (circles).

In our calculations the atmosphere is divided into about 45 layers. The actual number depends on the conditions at the ground. If the surface pressure is higher than 1000 hPa the boundaries of the lowest layer are fixed to surface pressure and 1000 hpa (then the next boundary is at 940 hPa) and, if not, then to surface pressure and 940 hPa. The further pressure differences between the boundaries of the layers are in succession from the bottom to the top (in hPa): 11×60, 2×30, 6×25, 9×10, 5×5, 2×2.5, 7×1, and as much steps of 0.5 hPa until the atmospheric pressure level of 1 hpa is reached.

Between two successive points of the given "real" atmosphere the conversion between height and pressure is done with the barometric height formula with the application of the virtual mean temperature. The temperature gradient is assumed to be constant and the air density is determined with the equation of state. The lapse rate of water vapor and ozone density are assumed to be exponential within each layer.

To facilitate the comparison of different radiation transfer models it is customary to use the model atmospheres given by McClatchey et al. (1978) for tropical, midlatitude summer and winter, and for subarctic summer and winter conditions. The profiles of temperature and the densities of air, vapor, and ozone are shown in Fig. 2.

3.2
Absorption Coefficients

The absorption coefficient k_ν of a single line is described by the product of the temperature dependent line strength S and the normalized line shape (see for instance Goody, 1964)

$$k_\nu = S(T) f(\nu - \nu_0) \ ,$$

where ν_0 is the wavenumber of the ideal monochromatic line. The strength of a line in dependence on temperature is given by

$$S(T) = S(T_0) \frac{Q_r(T_0)}{Q_r(T)} \frac{Q_v(T_0)}{Q_v(T)} \exp\{\frac{hc}{k} E(\frac{1}{T_0} - \frac{1}{T})\} \ . \qquad (11)$$

Here h and k are the Planck and Boltzmann constants, c is the velocity of light, E is the lower state energy, and Q_r, Q_v are the rotational and vibrational partition functions. After Herzberg (1945) the quotient of the rotational partition functions is approximately given by

$$\frac{Q_r(T_0)}{Q_r(T)} \approx (\frac{T_0}{T})^j \ .$$

The power j depends on the type of molecule. Values for j and the vibrational partition functions for special temperatures are listed in Table 2.

Table 2:
From McClatchey et al., 1973
with additional temperature dependence parameter n (Rothman et al.; 1987)

			Vibrational Partition Functions							
Molecule	j	Tempera-ture	175	200	225	250	275	296	325	n
H_2O	1.5		1.000	1.000	1.000	1.000	1.000	1.000	1.001	.64
CO_2	1.0		1.0095	1.0192	1.0327	1.0502	1.0719	1.0931	1.1269	.75
O_3	1.5		1.004	1.007	1.013	1.022	1.033	1.046	1.066	.76
N_2O	1.0		1.017	1.030	1.048	1.072	1.100	1.127	1.170	.75
CO	1.0		1.000	1.000	1.000	1.000	1.000	1.000	1.000	.69
CH_4	1.5		1.000	1.000	1.001	1.002	1.004	1.007	1.011	.75
O_2	1.0		1.000	1.000	1.000	1.000	1.000	1.000	1.001	.50

3.2.1
Absorption of Spectral Line Centres

For atmospheric conditions the process of forming the line shape is dominated by collisional damping and the Doppler effect. In general, absorption line profiles are asymmetric broadened and frequency shifted. However, there is no allbountiful solution to collisional broadening, especially not for the wings more than several wavenumbers away from the centre. But near the line centres pressure broadened line shapes are given by the Lorentz profile, where α_L is the halfwidth of the half peak intensity of the line.

$$k_\nu(p,T) = \frac{S(T)}{\pi} \frac{\alpha_L(p,T)}{(\nu-\nu_0)^2 + \alpha_L^2(p,T)} \tag{12}$$

At low pressures Doppler broadening from the Maxwell Boltzmann velocity distribution of molecules prevails. The convolution of the Lorentz and the Doppler profiles results in the Voigt profile (see for example Armstrong, 1967).

$$k_\nu(p,T) = k_0 \frac{y}{\pi} \int_{-\infty}^{+\infty} \frac{e^{-t^2}}{y^2 + (x-t)^2} dt \ , \tag{13}$$

where

$$k_0 = \frac{S(T)}{\alpha_D(T)}(\frac{\ln 2}{\pi})^{1/2} \ ,$$

$$y = \frac{\alpha_L(p,T)}{\alpha_D(T)}(\ln 2)^{1/2} \ , \qquad \text{and} \qquad x = \frac{\nu - \nu_0}{\alpha_D(T)}(\ln 2)^{1/2} \ .$$

The pressure–temperature dependent air-broadened Lorentz halfwidth and the temperature dependent Doppler halfwidth are given by

$$\alpha_L(p,T) = \alpha_L(p_0,T_0)\frac{p}{p_0}(\frac{T_0}{T})^n \quad \text{and} \quad \alpha_D = \frac{\nu_0}{c}(\frac{2kT}{m}\ln 2)^{1/2} \ , \qquad (14)$$

where the temperature dependence parameter n for different absorbers is listed in Table 2.

The Voigt line shape is only valid for collisional and Doppler broadening independent of each other. For high resolution spectroscopy deeper considerations may be necessary. Here is to mention the article of Herbert (1974) about collisional narrowing of the Doppler line shape which gives for the limit of soft collisions the Galatry profile. However, as Rodgers (1976) points out: for the most important absorbers in the atmosphere the maximum error in the equivalent widths of spectral lines comparing Voigt and Galatry profiles will not exceed 0.3 %. In the presence of the errors we have to tolerate in order to calculate fluxes and cooling rates by spectral and vertical integration this may be negligible.

The parameters of the individual spectral lines, i.e. position of the centre, line strength at given temperature, air-broadened Lorentz halfwidth at given temperature and pressure, and the lower state energy, which are required for computing absorption coefficients, are taken from the HITRAN database: 1986 edition (Rothman et al., 1987).

3.2.2
Absorption in the Wings of Spectral Lines

Various measurements have shown for the extreme wings of spectral lines that there is no sufficient accordance between calculated and measured absorption coefficients. Neither the dependence of the absorption coefficient on wavenumber nor its decrease with increasing temperature is reproduced accurately enough by theoretical shapes as discussed by Burch and Gryvnak (1980).

The behaviour of self and foreign broadened wings are different from each other and, according to Burch and Gryvnak, the total halfwidth for a binary collision at fixed temperature is given by

$$\alpha = \alpha_s^0 p_s + \alpha_f^0 p_f \ .$$

Here, normalized properties are denoted by the superscript 0, p_s is the partial pressure of the absorbing gas, and p_f is the one of the radiative inactive gas.

The total absorption coefficient in the range between absorption bands, called windows, then is given by

$$k = k(local) + C_s^0 p_s + C_f^0 p_f \ ; \tag{15}$$

where $k(local)$ is the absorption coefficient of lines lying in the window, C_s^0 and C_f^0 are the self and foreign broadening coefficients, respectively.

Finally, Eq. 15 leads to an expression for the continuum absorption coefficient

$$k_{Cont.}(\nu, p, p_s, T) \approx C_s^0(\nu, T)[p_s + \gamma(p - p_s)] \ , \tag{16}$$

where γ is the ratio of the foreign-broadening and the self-broadening coefficient, and p is the total pressure.

For the continuum absorption of water vapor in the window of 8 - 12 μm Roberts et al. (1976) found the empirical relation

$$\begin{aligned} C_s^0(\nu, T) &= C_*^0(\nu) \exp\{T_0(\frac{1}{T} - \frac{1}{296})\} \\ C_*^0(\nu) &= a + b \exp\{-\beta\nu\} \ , \end{aligned} \tag{17}$$

with the constants $a = 4.18\ cm^2 g^{-1} atm^{-1}$, $b = 557.8\ cm^2 g^{-1} atm^{-1}$, $\beta = 0.00787\ cm$, $\gamma = 0.001$, and $T_0 = 1800K$.

As Roberts et al. state, the estimation of γ is rather difficult and the value may be between 0 and 0.001 . The value of γ assumed to be constant means that the shapes for self and foreign broadening are the same.

No other continuum absorption than the one of water vapor at 10 μm is incorporated into the line-by-line model, because continuum absorption should only be important for high pressures and the absorption in the troposphere is dominated by water vapor. The continuum absorption of H_2O in the window at 4 μm is not incorporated, because there the blackbody radiation from the surface is small.

3.3
Integration of the Equation of the Differential Optical Thickness

It is evident from the discussion of the absorption coefficient that the integration of the general form of the differential optical thickness (Eq. 10) across a layer is not feasible. But if it is assured that the absorption coefficients do not vary with temperature and pressure within the layer too much, by keeping the layers small enough, we can assume that $k_\nu = \overline{k}_\nu$ is constant within each layer. Then, the difficulty of the integration of the optical thickness remains just a question of the assumptions made for the concentrations. The simplest case occurs for gases with constant concentrations. Here the integration can be performed at once and we receive

$$\tau_1 - \tau_2 = \overline{k}_\nu \frac{\overline{q}}{g}(p_1 - p_2) \ . \tag{18}$$

It would be easy to treat gases with variable concentrations the same by using an averaged concentration, but this is not necessary. If we assume that these concentrations are exponential dependent on height within each layer, which is more realistic especially for H_2O, and do the same for the air density,

$$\frac{d\ln q}{dz} := \frac{\Delta \ln q}{\Delta z} = h \ , \quad ; \quad \frac{d\ln \rho}{dz} := \frac{\Delta \ln \rho}{\Delta z} = r \tag{19}$$

then the integration can be performed analytically.

First we make use of the relation for the concentration and get

$$d\tau = \overline{k}_\nu \frac{q_2}{g} e^{h(z-z_2)} dp \ .$$

With the further assumption of the layers being in hydrostatic equilibrium

$$dp = -\rho g \, dz = -\rho_2 g e^{r(z-z_2)} dz \ , \tag{20}$$

it is

$$[-\frac{r}{\rho_2 g}(p - p_2) + 1]^{h/r} = e^{h(z-z_2)} \ . \tag{21}$$

Using the substitutions

$$a = -\frac{r}{\rho_2 g} \ ; \ n = \frac{h}{r} \ ; \ b = -ap_2 + 1 \ ; \ D = a(p_1 - p_2) + 1$$

the integral equation for the optical thickness can be rewritten.

$$\int_{\tau_2}^{\tau_1} d\tau = \int_{p_2}^{p_1} \overline{k}_\nu \frac{q_2}{g} [ap' + b]^n \, dp' \tag{22}$$

Finally, paying attention to two cases the difference of the optical thickness at the boundaries of the layer is found.

$$n \neq -1: \quad \tau_1 - \tau_2 = \overline{k}_\nu \frac{q_2}{g} \frac{1}{a(n+1)} (D^{n+1} - 1) \tag{23}$$

$$n = -1: \quad \tau_1 - \tau_2 = \overline{k}_\nu \frac{q_2}{g} \frac{1}{a} \ln(D) \tag{24}$$

To derive the formula of the optical thickness for the case of H_2O continuum absorption equations (10) and (16) are combined to

$$d\tau = C_s^0(\nu, T)\{e + \gamma(p - e)\} \frac{q}{g} dp \ . \tag{25}$$

This time only the assumption that the absorption coefficients are constant with respect to temperature within the layer have to be made. However, the dependence on pressure can be explicitly considered. Again using the assumptions of exponential dependences of the concentration and the air density on height and additionally with the partial water vapor pressure $e \approx qp/0.622$, there is similar to the above

$$\tau_1 - \tau_2 \approx s(1-\gamma) \int_{p_2}^{p_1} p'[ap' + b]^{2n} \, dp' + t \int_{p_2}^{p_1} p'[ap' + b]^n \, dp' \ , \tag{26}$$

with using the expressions

$$s = C_s^0(\nu, \overline{T}) \frac{q_2^2}{0.622 g} \quad \text{and} \quad t = C_s^0(\nu, \overline{T}) \frac{\gamma q_2}{g} \ .$$

Now paying attention to four cases the difference of the optical thickness at the layer boundaries are received (Eq. (27), (28) , (29), and (30)).

$n \neq -1 \ , \neq -2 \ , \neq -\frac{1}{2}$

$$\begin{aligned} \tau_1 - \tau_2 \ \approx \ & \frac{s(1-\gamma)}{a^2} \{ \frac{1}{2n+2} (D^{2n+2} - 1) - \frac{b}{2n+1} (D^{2n+1} - 1) \} \\ & + \frac{t}{a^2} \{ \frac{1}{n+2} (D^{n+2} - 1) - \frac{b}{n+1} (D^{n+1} - 1) \} \end{aligned} \tag{27}$$

$n = -1:$

$$\begin{aligned} \tau_1 - \tau_2 \ \approx \ & \frac{s(1-\gamma)}{a^2} \{ \ln(D) + b(\frac{1}{D} - 1) \} \\ & + \frac{t}{a^2} \{ a(p_1 - p_2) - b \ln(D) \} \end{aligned} \tag{28}$$

$n = -2:$

$$\begin{aligned} \tau_1 - \tau_2 \ \approx \ & \frac{s(1-\gamma)}{a^2} \{ \frac{1}{2n+2} (D^{2n+2} - 1) - \frac{b}{2n+1} (D^{2n+1} - 1) \} \\ & + \frac{t}{a^2} \{ \ln(D) + b(\frac{1}{D} - 1) \} \end{aligned} \tag{29}$$

$n = -\frac{1}{2}$:

$$\tau_1 - \tau_2 \approx \frac{s(1-\gamma)}{a^2}\{a(p_1 - p_2) - b\ln(D)\} + \frac{t}{a^2}\{\frac{1}{n+2}(D^{b+2} - 1) - \frac{b}{n+1}(D^{n+1} - 1)\} \quad (30)$$

Although the determination of the optical thickness proposed here seems to be intricate, it is not time consuming in a model run, because it can be precalculated once for all layers. Only the coefficients $\overline{k}_\nu$ and $C_s^0(\nu, \overline{T})$ have to be inserted at each wavenumber point.

3.3.1
Numerical Aspects of the Calculation of the Absorption Coefficients

The direct integration of the Voigt profile (Eq. 13) is very time expensive. Several approximation algorithms have been proposed, where the one by Armstrong (1967) is the most accurate, taking advantage of the coherency of the Voigt profile and the complex probability function. Drayson (1976) and Pierluissi et al. (1977) have proposed algorithms proceeding from Armstrong's one, which are faster but less accurate. Other methods with partly intuitive assumptions have been developed by Whiting (1968) and Matveyev (1972).

Computer runs have been made to compare the calculation times and the accuracies of the mentioned approximations. For this purpose all algorithms were put into seperate FORTRAN subroutines where the codes given by Armstrong and Drayson were modified by using those parts one time which are only needed for the initialization (The FORTRAN DOUBLE PRECISION statements were disabled).

We chose an artificial spectral line at $\nu_0 = 2400$ cm^{-1} and measured the calculation time of each algorithm (inclusive calling the subroutine) starting at the line centre until the distance $\Delta\nu$=1 cm^{-1} from the line centre was reached. Two runs for T = 300 K were made, the one with p = 1 hPa and the other with p = 1000 hPa. In Table 3 the quotient of the calculation time of each algorithm, related to the time Armstrong's code needed, can be seen.

In Fig. 3 the accuracy that each algorithm yields is shown in dependence on the distance from the line centre. The absorption coefficients are compared with those obtained by Armstrong's code. We see that the algorithm of Drayson agrees very well in any distance to the line center, the one by Pierluissi et al. likewise, but with the exception of a narrow range about $\Delta\nu = .014$ cm^{-1} , where the deviation

reaches up to −28 %. Hence, the algorithm of Drayson is used in our line-by-line model to calculate the absorption coefficients of the central range of spectral lines.

Table 3:
Comparison of Voigt Profile Calculation Algorithms.
Quotient of running time related to Armstrong's code.

Authors	at p = 1 hPa	at p = 1000 hPa
Armstrong (1968)	1.000	1.000
Drayson (1976)	0.403	0.334
Pierluissi et al. (1977)	0.459	0.271
Matveyev (1972)	0.607	0.701
Whiting (1968)	0.402	0.448
Lorentz profile	0.151	0.174

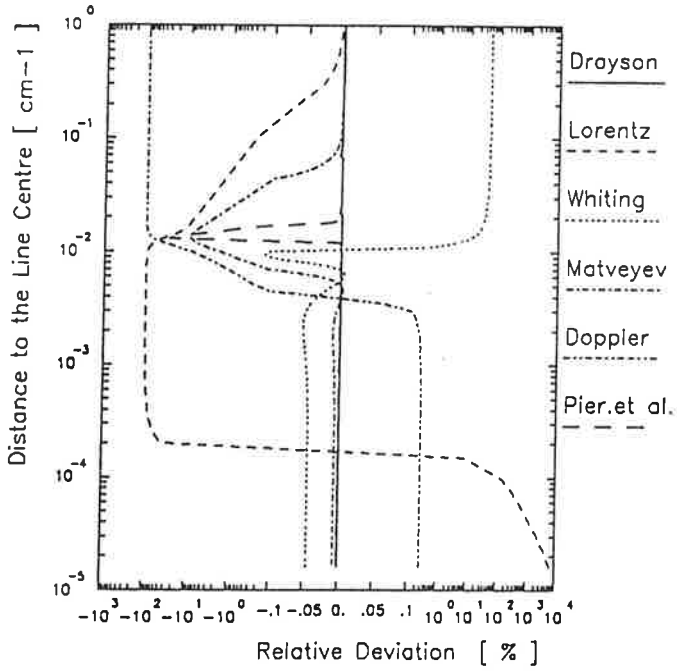

Fig. 3: Comparison of different codes for approximating the Voigt shape related to the one of Armstrong (1967) as function of the distance from the line centre.

If we consider the time differences between Drayson's code and the Lorentz profile we notice that the usage of the Lorentz profile is advantageous whenever it is possible. From Fig. 3 it is evident that the Lorentz profile yields very good accuracy for distances of 1 cm^{-1} and more from the centre, where the asymptotic approach has already occured.

In order to obtain the worst possible error in using the Lorentz profile instead of the Voigt profile, the atmospheric and spectral conditions have been chosen such that the asymptotic approach of both profiles should be as far as possible from the line centre. This occurs for high temperature, low pressure, and high frequency. In this context the dependence on Lorentz halfwidth does not play an important part.

Artificial absorption lines have been created by chosing for each of the seven main absorbers such spectral ranges, which correspond to the line positions in the most shortwave band of the absorbers in the IR. Results for T = 320 K and p = 1 hPa are shown in Fig. 4 .

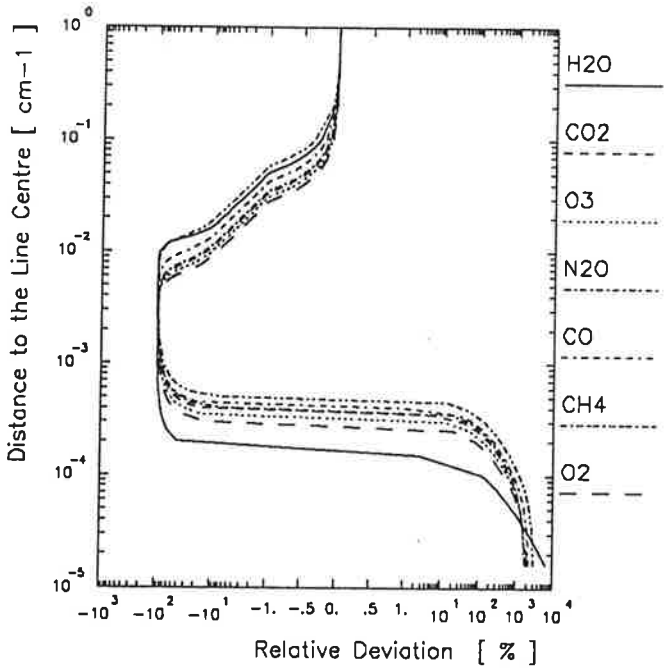

Fig. 4 : Relative deviation of the Lorentz profile from the Voigt profile for the denoted molecules as function of the distance from the centres of artificial absorption lines with line positions taken from Table 4.

The distances from the artificial line centres for each absorber, for which the relative deviations between the Lorentz and the Voigt profile wings are less than 1 % are listed in Table 4. For distances greater than these the Lorentz profile is used in our line-by-line model instead of the Voigt profile.

Table 4: Explanations see text

	ν_0 [cm^{-1}]	$\Delta\nu$ [cm^{-1}]
H_2O :	2300	.052
CO_2 :	2400	.036
O_3 :	2300	.032
N_2O :	2500	.036
CO :	2400	.044
CH_4 :	2500	.060
O_2 :	1700	.030

4
Spectral Resolution

The accuracy of evaluating fluxes and cooling rates depends not only on the calculation of the absorption coefficients but on an appropriate spectral resolution, too. Two ways of influencing the resolution are considered: varying the division of the whole spectrum and changing the order of the numerical integration scheme.

4.1
Division of the IR

The simplest way to handle resolution is to divide the IR into very small intervals with constant width. If, for example, a trapezoid integration scheme would be applied and it should be assured that the central part of each line is represented at least by two points even in the stratosphere, then a width of $\approx 10^{-4}$ cm^{-1} for long wavelengths and somewhat more for shorter wavelengths (because of the dependence of the Voigt halfwidth on frequency) should be used. For the whole IR this would result in a few millions of subintervals.

In order to reduce the number of subintervals larger constant steps could be used, but then many line centres could be missed which should result in considerable errors. However, to obtain a line-by-line model with a reduced number of subintervals a resolution scheme was developed which takes the spectral distribution of the absorption lines into account.

For each absorbing gas in a calculation the positions of the line centres are looked up, then the Voigt halfwidths at atmospheric conditions at about 50 Km height are evaluated. All spectral points with the distance of the Voigt halfwidth to each centre are calculated, and sorted in ascending spectral sequence.

If we suggest the line cores to have rectangular shapes, as noted similar by Fels (1979), the widths of the central part of isolated lines in the upper part of the stratosphere are approximately known. The double of the Voigt halfwidths, which are given approximately by Eq. 31 (Posener; 1959), equals the widths of the cores.

$$\alpha_V \approx (\alpha_L^2 + \alpha_D^2)^{\frac{1}{2}} \tag{31}$$

(The notion of rectangular cores to be independent on pressure works best for high frequencies. However, in the IR the line cores get much broader with increasing pressure, especially for the rotational water vapor lines).

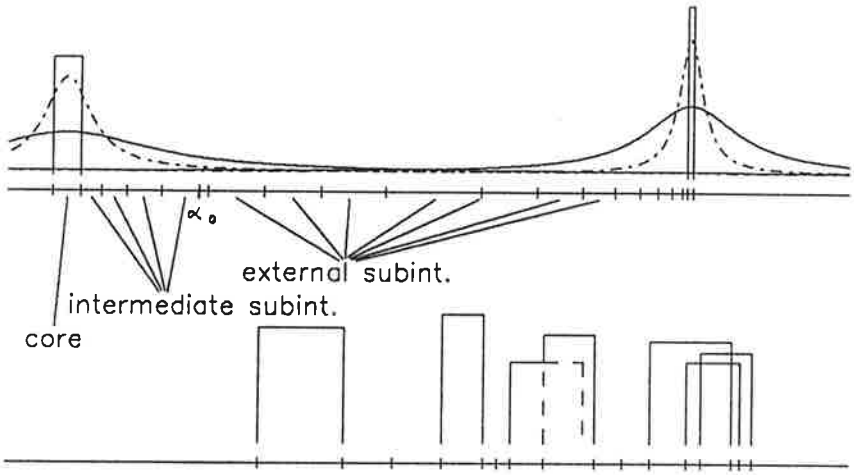

Fig. 5: Spectral intervals and the distribution of the subinterval types within the resolution scheme dependent on the spektral lines distribution (DLD).

When sorting the spectral points flags are set for isolated lines, two overlapping lines, or clusters of more than two overlapping lines where the latter are rare in the IR. The number of points are reduced by omitting one of the four points of only two lines being overlapped. Here, the stronger line gets the full width of its line core, the rest interval remains for the weaker line. For clusters of lines on

contrary, all spectral points are used without reducing the number according to the line strengths.

If two neighbouring cores do not overlap, the range between them is split into two parts and subdivided as follows: The left and right most subintervals are obtained by incrementing the logarithms of the corresponding Voigt halfwidths by a constant amount. The following subintervals are enlarged by incrementing the logarithm of the preceding ones. This is done until the middle of the range is reached (the remaining 'incomplete' subinterval is added to the last). However, it is assured that no subinterval exceeds the width of 0.1 cm^{-1} .

Of course, the determination of the widths of the cores are not restricted solely to the double of the Voigt halfwith as described above. So, a higher resolution scheme is achieved by setting the widths of the cores equal to the double of the Lorentz halfwidths at low pressure.

Calculations were made to compare the described resolution scheme (Depending on the spectral Lines Distribution: DLD resolution) with the resolution with constant steps of 10^{-2} and 10^{-3} cm^{-1} in three distinct spectral ranges: part of the rotational band of water vapor (400 - 410 cm^{-1}; only H_2O lines were considered), part of the 15 μm band of CO_2 (620 - 630 cm^{-1} ; CO_2 and H_2O), and part of the 9.6 μm ozone band (1000 - 1010 cm^{-1}; O_3, CO_2 , and H_2O with continuum absorption).

Fig. 6: Comparison of spectral resolutions: Relative deviations of the downward flux densities (left) and cooling rates (right) derived with constant steps of 0.001 cm^{-1}(solid curve), the DLD resolution with the application of the Voigt halfwidths as half cores (dashed curve), and the usage of constant steps of 0.01 cm^{-1} (pointed curve) from the DLD resolution scheme with the application of the Lorentz halfwidths at p = 1 hPa and T = 296 K as half cores. For each subinterval an eight point Gaussian quadrature is applied.

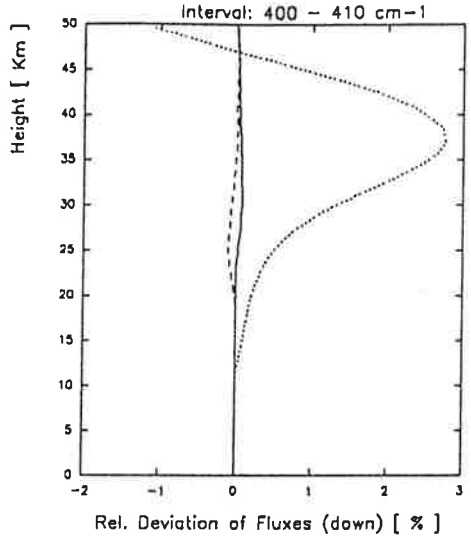
Interval: 400 - 410 cm-1
Height [Km]
Rel. Deviation of Fluxes (down) [%]

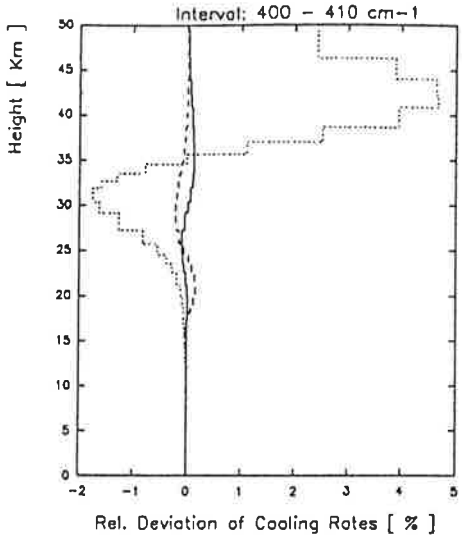
Interval: 400 - 410 cm-1
Height [Km]
Rel. Deviation of Cooling Rates [%]

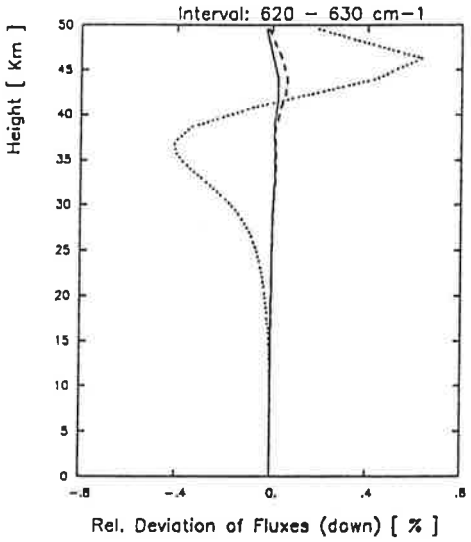
Interval: 620 - 630 cm-1
Height [Km]
Rel. Deviation of Fluxes (down) [%]

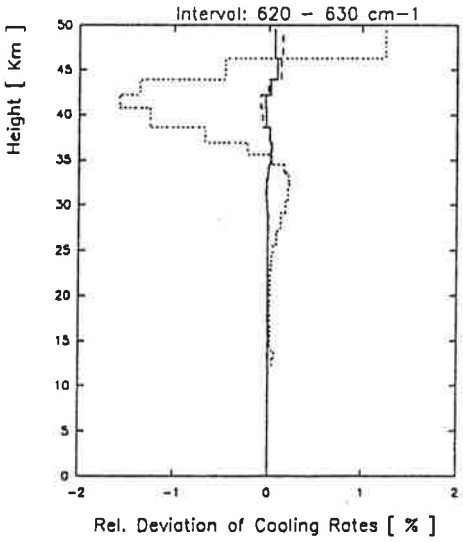
Interval: 620 - 630 cm-1
Height [Km]
Rel. Deviation of Cooling Rates [%]

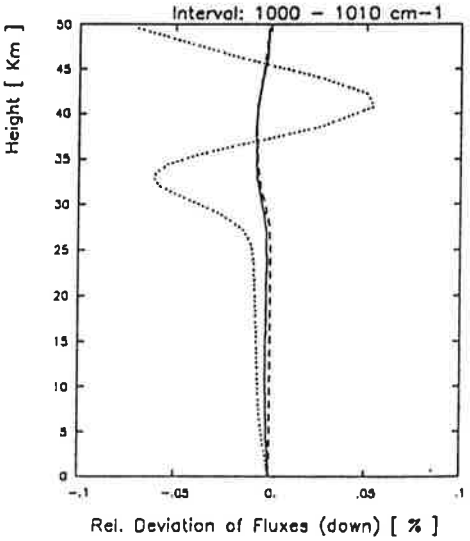
Interval: 1000 - 1010 cm-1
Height [Km]
Rel. Deviation of Fluxes (down) [%]

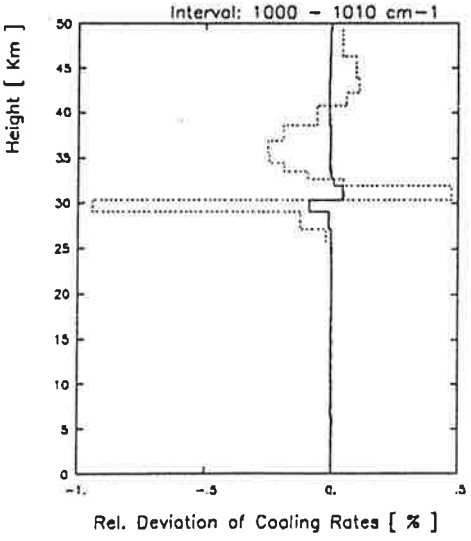
Interval: 1000 - 1010 cm-1
Height [Km]
Rel. Deviation of Cooling Rates [%]

All lines were cut off at the distance $\Delta\nu = 10$ cm^{-1} from the line centres. For the integration over the cosine of the zenith angle a four point and for the spectral integration an eight point Gaussian quadrature was applied. And the midlatitude summer atmosphere was used.

Fig. 6 shows the deviations for the downward total flux densities and for the cooling rates produced by the DLD scheme with the application of the Voigt halfwidths as half cores, by the scheme with constant steps of 0.01 cm^{-1}, and by the scheme with constant steps of .001 cm^{-1} from those of the DLD scheme with the application of the Lorentz halfwidths at about 50 Km height as half cores.

Good agreement between all schemes is exhibited within the atmosphere, with the exception of the resolution by constant steps of 0.01 cm^{-1} within the stratosphere. The largest deviations of the scheme with the broader constant steps (pointed) appear in the range of the rotational water vapor band (400 - 410 cm^{-1}). However, it is known that IR fluxes and cooling rates in the stratosphere are dominated by CO_2, so the larger deviations for the rotational water vapor band within the stratosphere are negligible. The maximum deviations of the flux densities within the stratosphere of less than 0.5 % and the cooling rates of less than 1.5 % for the range 620 – 630 cm^{-1} seem tolerable.

4.2
Varying the Order of the Spectral Gaussian Quadrature

As mentioned before the accuracy of calculated fluxes and cooling rates is affected by the order of the numerical integration scheme. In order to reduce computation time without losing too much accuracy we want to avoid using a quadrature of high order when it is not necessary. The line-by-line model with DLD resolution distinguishes three spectral ranges: line cores, intermediate subintervals, and external subintervals. Here, as indicated in Fig. 5, intermediate subintervals are located in the range extending from the core to the spectral point where the Lorentz halfwidth (at 1 atm and T = 296 K) is reached. External subintervals then lie between the spectral positions of the Lorentz halfwidths at p = 1 atm of two adjacent lines.

For each of these interval types different orders of the numerical integration of the DLD scheme with the application of the Voigt halfwidths as half cores were tested. As reference the flux densities and cooling rates calculated with an eight point Gaussian quadrature in each of the three interval types are used. Retaining all computational settings and the eight point in the respective other ranges now a five point quadrature for the cores (solid curve in Fig. 7), for the intermediate subintervals (dashed curve), and for the external subintervals (pointed curve) is applied.

From Fig. 7 it is evident that sensitivity is highest in the intermediate subintervals. This is quite reasonable because here the transition from line core behaviour to wing behaviour is found, if we go through the atmosphere from the ground to the top. If very accurate fluxes are needed, an eight point quadrature is recommended here. However, deviations of less than 0.5 % of downward flux densities and of less than 0.7 % of cooling rates within the stratosphere should be sufficient in most cases.

The interval between 400 - 410 cm^{-1} is the only one in which the influence of varying the order of quadrature in the external subintervals can be examined because in the other two ranges external subintervals are too scarce. There it seems that the five point quadrature is sufficient enough.

For the core range, there are larger deviations only in the interval within the ozone band. However, the maximum of relative deviations of the cooling rates occurs where a change from cooling to heating happens and the absolute values of the cooling rates in 30 Km height are rather small.

Finally, the application of a two point Gaussian quadrature for the cores within the DLD scheme with the Lorentz halfwidths as half core widths gives sufficient results (maximum relative deviation of - 0.1 % for the downward flux densities within the stratosphere). However, for this resolution scheme the number of subintervals is higher.

Fig. 7: Variation of the number of points for the Gaussian quadrature (npG) with the denotation npG(core, intermediate subintervals, external subintervals) : solid curves with npG(5,8,8); dashed curves with npG(8,5,8); pointed curves with npG(8,8,5).

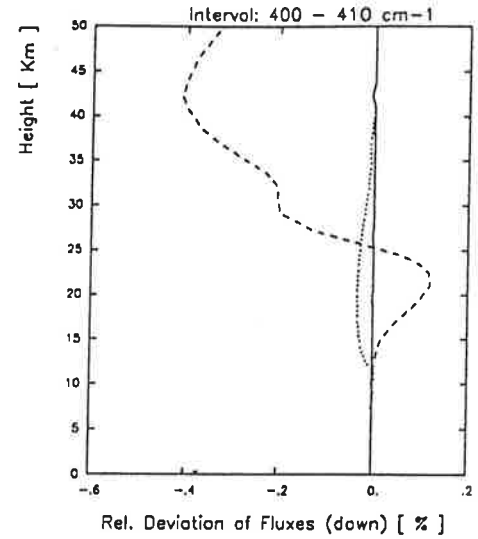
Interval: 400 - 410 cm-1
Height [Km]
Rel. Deviation of Fluxes (down) [%]

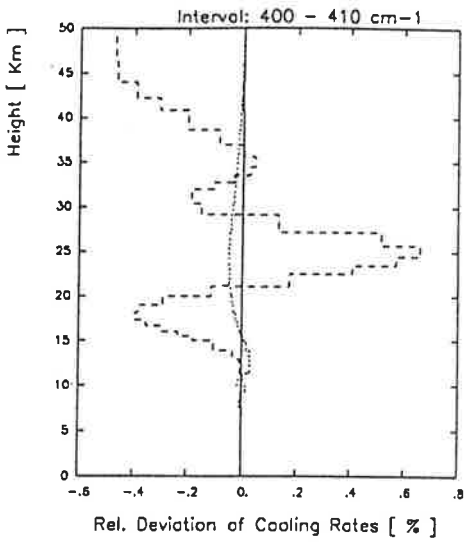
Interval: 400 - 410 cm-1
Height [Km]
Rel. Deviation of Cooling Rates [%]

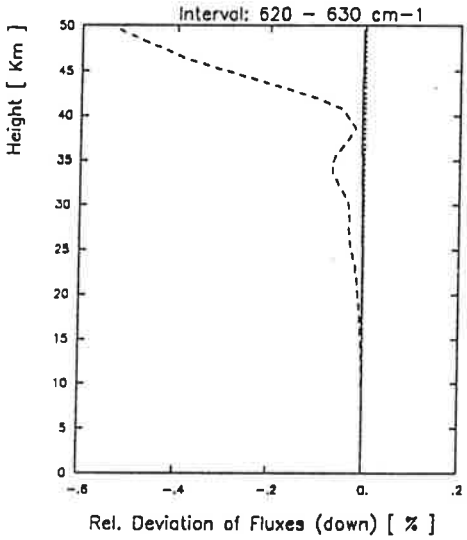
Interval: 620 - 630 cm-1
Height [Km]
Rel. Deviation of Fluxes (down) [%]

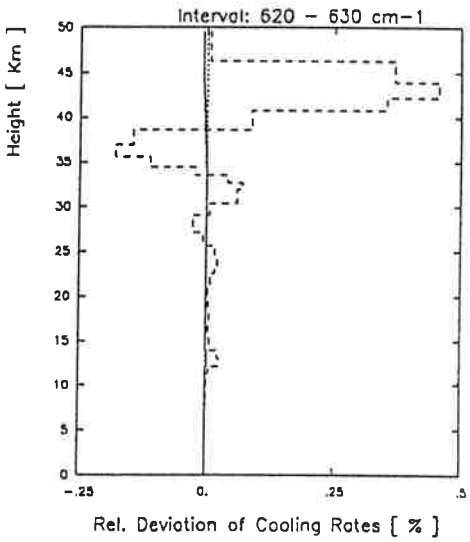
Interval: 620 - 630 cm-1
Height [Km]
Rel. Deviation of Cooling Rates [%]

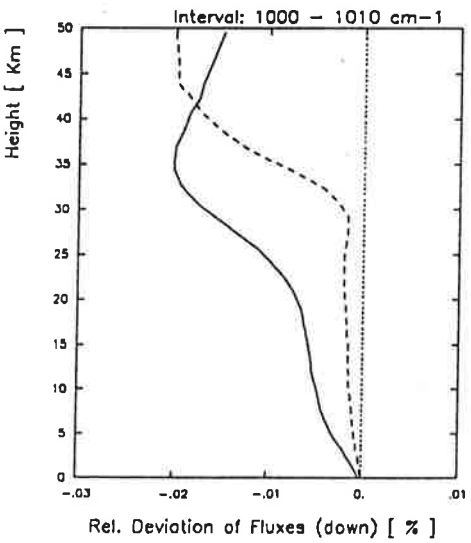
Interval: 1000 - 1010 cm-1
Height [Km]
Rel. Deviation of Fluxes (down) [%]

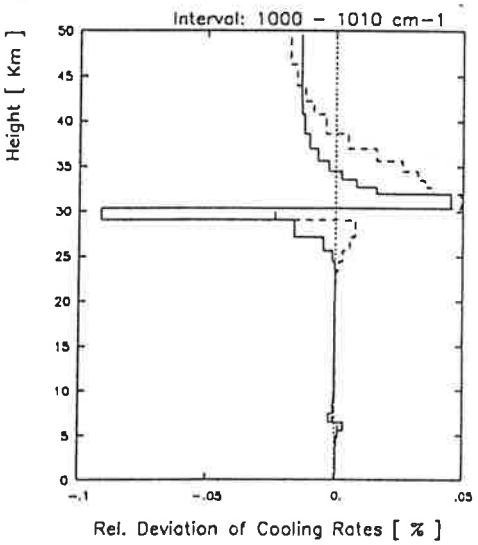
Interval: 1000 - 1010 cm-1
Height [Km]
Rel. Deviation of Cooling Rates [%]

4.3
Flux Densities and Cooling Rates in the Range of 1100 to 1500 cm^{-1}

In this section the comparison between the spectral resolution scheme of dividing the IR into constant subintervals (0.01 cm^{-1} width) and the DLD resolution scheme is applied on the spectral range 1100 – 1500 cm^{-1}. Within the DLD scheme Gaussian quadrature has been applied with three points for the line cores (which widths equal the double of the Lorentz halfwidths at p = 1 hPa), eight points for the intermediate subintervals, and five points for the external subintervals. This spectral interval is chosen, because here intricate overlapping of absorption bands is found. Considerable absorbers are H_2O (with continuum absorption), O_3 , CH_4 , and N_2O.

Flux densities and cooling rates were calculated for a midlatitude summer atmosphere with both resolution schemes.

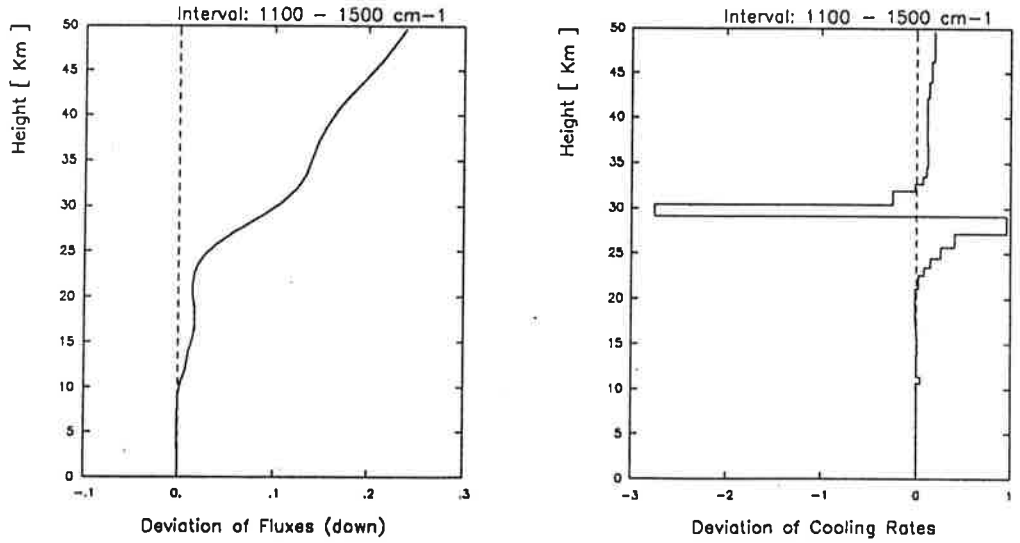

Fig. 8: Relative deviations (solid curves) in % and absolute deviations (dashed curves) in W/m^2 for the downward flux densities and K/d for the cooling rates with the application of the spectral resolution with 0.01 cm^{-1} constant width and the DLD resolution scheme with the application of the Lorentz halfwidths at p = 1 hPa and T = 296 K as half of the widths of the cores.

In Fig. 8 the relative deviations of downward flux densities (left picture) and cooling rates (right) are drawn as solid curves and the dashed ones represent the absolute deviations. The absolute deviations for the cooling rates and for the downward are almost vanishing, so there is no need to be concerned with the relative deviations. Not shown are the upward flux densities, because even the relative deviations are almost vanishing.

These results seem to justify to use the constant step width 0.01 cm^{-1} in conjunction with the eight point Gaussian quadrature in any spectral range of the IR.

5

Calculation of Flux Densities and Cooling Rates in the IR

For the following calculations the same settings in our line-by-line model will be retained:

The inclusion of the Voigt line shape is approximated as discussed in section 3.3.1 and all absorption lines are cut off at the distance of 10 cm^{-1} from the line centres.

In the atmospheric window between 8 μm and 14 μm the water vapor continuum absorption according to Roberts et al. (1976) is included additionally to the line-by-line absorption coefficient.

For the numerical integration over the cosine of the zenith angle a four point Gaussian quadrature is used.

The atmosphere is divided into layers with the pressures at the boundaries mentioned in section 3.1 . The densities of water vapor and ozone are taken from the applied model atmosphere and for the gases with constant concentrations the following values are used: CO_2: 300 ppmv; N_2O: 0.28 ppmv; CO: 0.75 ppmv; CH_4: 1.75 ppmv, and O_2: 20.95 %.

The evaluation of the optical thickness for gases with constant concentrations is carried out according to Eq. (18), the one for water vapor and ozone line absorption with the assumption of the concentrations being exponential dependent on height within a layer according to Eq. (23) and (24), and for the water vapor continuum according to equations (27) to (30).

5.1
Comparison of Flux Densities with the ICRCCM Study

The mentioned settings facilitate the comparison of calculated flux densities with those recorded in the ICRCCM study (the InterComparison of Radiation Codes in Climate Models; WMO 1984). In this study, among other things, the results of several line-by-line models have been compared with each other for various atmospheric states and absorbers. The comparison with results of our own model is restricted to flux densities in a midlatitude summer atmosphere with absorption by a) H_2O lines only, b) CO_2 lines only, c) O_3 lines only, and d) with total absorption in the IR by CO_2, O_3, H_2O (with continuum), CH_4, and N_2O.

From Table 5 it is evident that there is good agreement between all line-by-line models, if the lines of only one absorber (for CO_2 the adjusted flux densities have to be compared, see footnotes 6 and 7) are considered seperately. Only in the case of the 14 μm ozone band the flux densities show a discrepancy between the ICRCCM study and our own results. However, as already suggested in the study, the line-by-line models use different line parameter compilations. Since the AFGL 1980 edition used by GLAS and GFDL and the edition from 1986 used in our model several updates and inclusions of new bands for ozone have taken place. Finally, the fact that the sum of the (own) flux densities of both bands (5.76 W/m^2) deviates from the value of the (own) flux densities for the whole IR (5.86 W/m^2) is due to ozone absorption lines out of the 9.6 and 14 μm bands.

The comparison of fluxes for the case of water vapor lines shows that the agreement between our own model and the one of GLAS is much better than with LMD. This is probably due to the fact that GLAS and our model performed for the shown results angular integration and a strict cut off of all lines at the distance of 10 cm^{-1}. Whereas the LMD model applies the diffusivity factor D=1.66 and the cut off criterion $800 \times \alpha_L$. Hence, in the LMD model the cut off distance for water vapor lines in the lower troposphere is up to 80 cm^{-1}.

Table 5
Comparison of flux densities from the ICRCCM study with own calculations

Source	$F^{up}_{surface}$	$F^{down}_{surface}$	$F^{net}_{surface}$	$F^{up}_{trop.}$ [1)]	$F^{down}_{trop.}$	$F^{net}_{trop.}$	F^{up}_{top}
From Table 2: Line-by-line flux calculations (W/m^2) for CO_2 only. Midlatitude Summer, 300 ppmv CO_2							
GISS[2)]	423.57	75.36	348.21		371.49		384.33
GFDL[3)]	423.57	75.38	348.19		371.96		384.54
LMD[4)]	423.57	76.38	347.19		371.04		383.52
own[6),7)]	423.56	75.85	347.75		371.35		384.15
own[8)]	422.81	75.85	347.00		370.60		383.40
From Table 5: Line-by-line flux calculations (W/m^2) for O_3 only. Midlatitude Summer, 9.6 μm + 14 μm bands							
GLAS[5)]	423.48	5.92	417.56		416.54		412.06
GISS	423.56	6.37	417.19		416.03		411.70
GFDL	421.37	6.07	415.30		414.31		409.82
LMD[9)]	420.98	4.99	415.98		414.43		411.56
own[10)]	422.81	5.86	416.94		416.05		412.06
own[11),12)]		5.76					
9.6 μm band only							
GLAS		4.40					
GISS		4.79					
GFDL		4.43					
LMD		4.41					
own		4.39					
14 μm band only							
GLAS		1.50					
GISS		1.58					
GFDL		1.53					
own[12)]		1.37					

Table 5: continuation

Source	$F^{up}_{surface}$	$F^{down}_{surface}$	$F^{net}_{surface}$	$F^{up}_{trop.}$	$F^{down}_{trop.}$	$F^{net}_{trop.}$	F^{up}_{top}
From Table 4: Line-by-line flux calculations (W/m^2) for H_2O (lines only). Midlatitude Summer; interval: 100 – 2600 cm^{-1}							
LMD	420.98	267.29	153.69			324.71	329.51
GLAS	420.97	263.25	157.73			328.93	334.61
own	420.94	263.64	157.30			328.25	334.82
From Table 8: Line-by-line calculations for midlatitude summer atmosphere including CO_2 , O_3 , H_2O (with continuum), CH_4 and N_2O . The LMD results are for 300 ppmv CO_2 , whereas the GLAS results are for 330 ppmv. The spectral interval 100-2600 cm^{-1} was used in all calculations.							
LMD	421.00	341.80	79.20	288.30	20.70	268.00	284.00
GLAS	421.00	341.30	79.60	288.90	21.20	267.80	283.30
own[13]	420.94	342.37	78.57	290.13	21.43	268.70	285.70
(Continuum absorption in the interval 8 – 14 μm)							
own	420.94	329.81	91.13	291.56	21.60	269.96	287.10
(Continuum absorption in the interval 8 – 12 μm)							

1) Tropopause at 13 Km or 179 hPa

2) Goddard Institute for Space Studies, New York. Spectral range: calculation dependent

3) Geophysical Fluid Dynamics Laboratory, Princeton. Spectral range: 0 - 2200 cm^{-1}

4) Laboratoire de Meteorologie Dynamique, Paris. Spectral range: 100 - 2600 cm^{-1}

5) Goddard Laboratory for Atmospheres, Greenbelt, Maryland. Spectral range: 0 - 3000 cm^{-1}

6) settings for the own calculations as described in the text
spectral range: calculation dependent; used here: 10 - 2500 cm^{-1}

7) The results of the GFDL and LMD upward and net fluxes have been adjusted to those which the various models would compute for the interval $\nu = 0$ to ∞, and so we did with our own results

8) pure results without adjustment

9) LMD results include only partially the contribution of the 14 μm band

10) application of all lines in the IR

11) only for the sum of the 9.6 μm and 14 μm bands contributions

12) GLAS and GFDL used AFGL line parameters from the 1980 edition. However, in the 1982 edition a new band has been included (Rothman et al., 1983), and in the 1986 compilation several updates took place

13) own calculation with 300 ppmv CO_2

In comparing the flux densities calculated with the consideration of all lines and the inclusion of the water vapor continuum absorption there is to state that the fluxes of our model are larger than those of LMD and GLAS for both directions at any level (except the upward flux at the surface). The largest differences are found between GLAS and our model for F_{top}^{up} with 2.4 W/m^2. However, this is quiet understandable, because the larger CO_2 concentration used in the GLAS model reduces upward flux densities. The largest percentage deviation is found at the tropopause for the downward flux between LMD and our model with about 3.5 %.

Faced with the differences of about 4 W/m^2 at any level between GLAS and LMD for H_2O (lines only) absorption and the different treatment of the line cut off, the agreement between both models for including all absorbers seems amazing. Therefore, it is difficult to understand the reason for the remaining differences of flux densities.

Finally, the comparison of own fluxes calculated with the inclusion of water vapor continuum absorption in the spectral interval 8 – 14 μm with those for the interval 8 – 12 μm demonstrates the importance of absorption by far wings of water vapor lines.

5.2
Dependences of Flux Densities and Atmospheric Cooling Rates on the Degree of Overlapping of Absorption Bands

For estimating the influence of overlapping of absorption bands in spectral subranges, the absorption coefficients at STP for the seven main absorbers in the IR for the case of a midlatitude summer atmosphere have been calculated. The IR has been divided corresponding to the vertical dashed lines of Fig. 9 according to the presence of overlapping absorption bands. The horizontal dashed part for H_2O denotes the continuum absorption range.

Calculations were carried out with subintervals of constant spectral resolution of 10^{-2} cm^{-1} because of two reasons: firstly, this scheme needs much less computation time than the DLD resolution scheme and secondly, only the resolution with constant steps allows to calculate the transmission for each absorber separately and to evaluate the transmission for the case of overlapping bands by multiplying the single transmissions. (As mentioned before the DLD resolution scheme depends on the spectral distribution of the lines, so that the calculation

of transmissions for each single absorber and the combination of absorbers would need its own computation run.)

The resulting downward total flux densities are shown in Fig. 10 and the atmospheric cooling rates in Fig. 11 for the subintervals a - p as indicated in Fig. 9. Taking into account the magnitudes of the resulting flux densities and cooling rates we notice that for some subintervals overlapping of bands is negligible, for others the overlapping of only two bands has to be considered, and only for the range between approximately 1000 - 1300 cm^{-1} intricate overlapping might be considered.

Fig. 9: Division of the IR according to the distribution of the absorption bands. The horizontal dashed part for H_2O denotes the continuum absorption range.

	cm^{-1}		μm		cm^{-1}		μm		cm^{-1}		μm
	10	~	1000.0		870	~	11.5		1500	~	6.7
a				f				k			
	220	~	45.5		950	~	10.5		1700	~	5.9
b				g				l			
	560	~	17.9		1100	~	9.1		1900	~	5.3
c				h				m			
	650	~	15.4		1240	~	8.1		2200	~	4.5
d				i				n			
	833	~	12.0		1350	~	7.4		2300	~	4.3
e				j				o			
	870	~	11.5		1500	~	6.7		2400	~	4.2
								p			
									2500	~	4.0

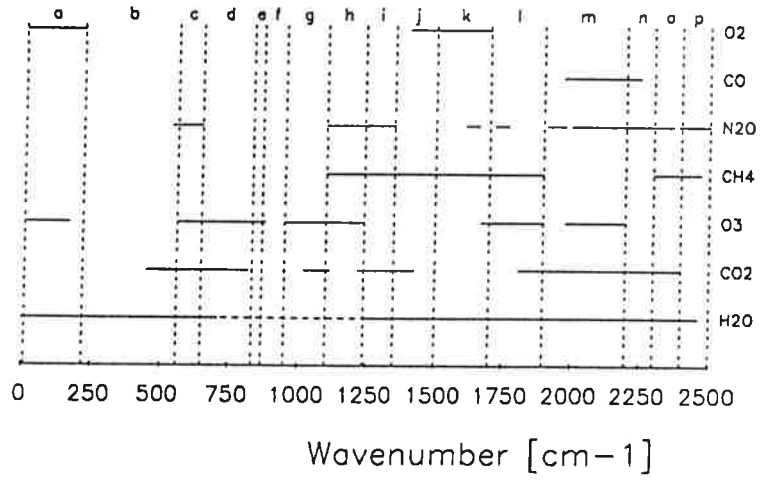

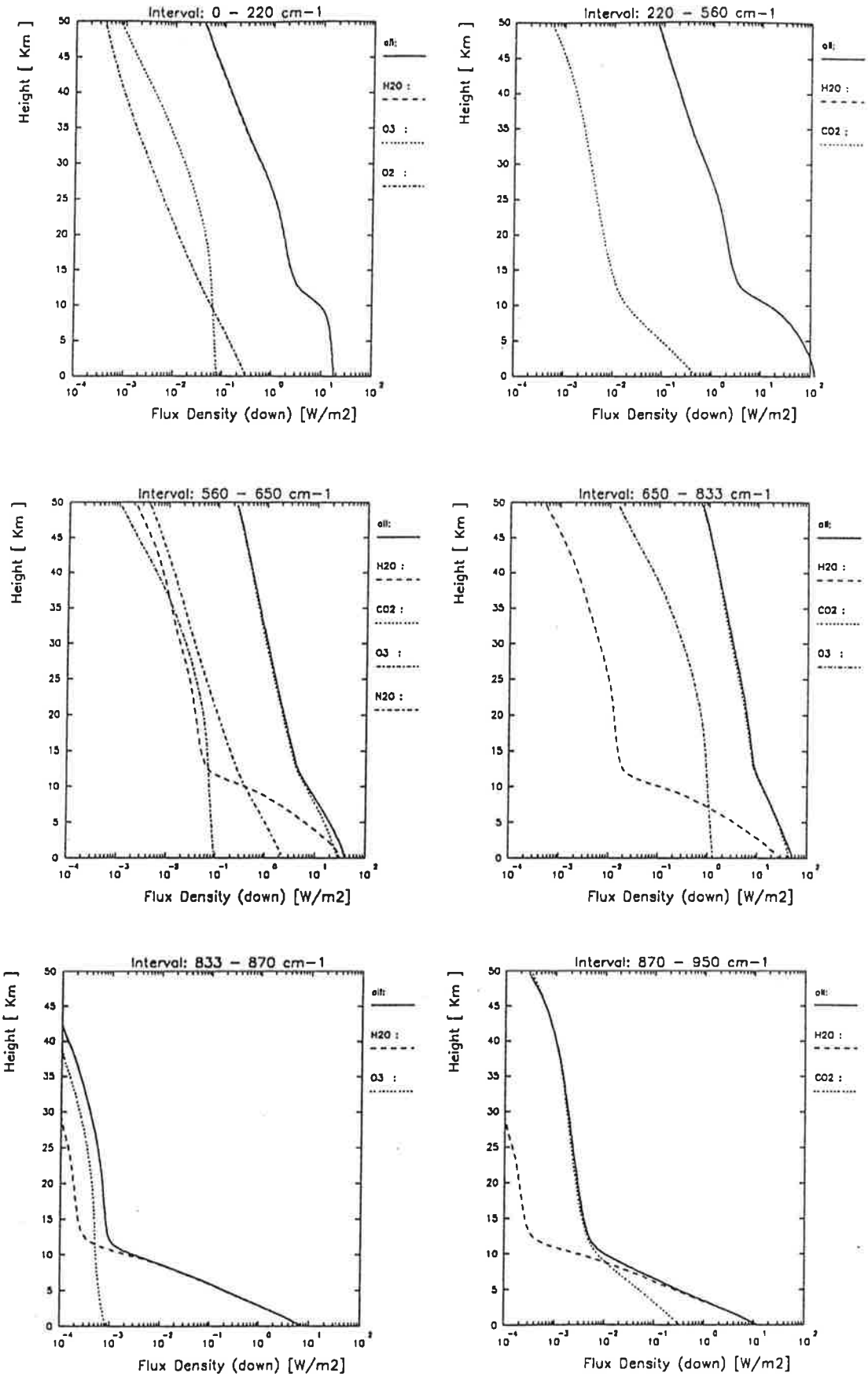

Fig. 10 : continued

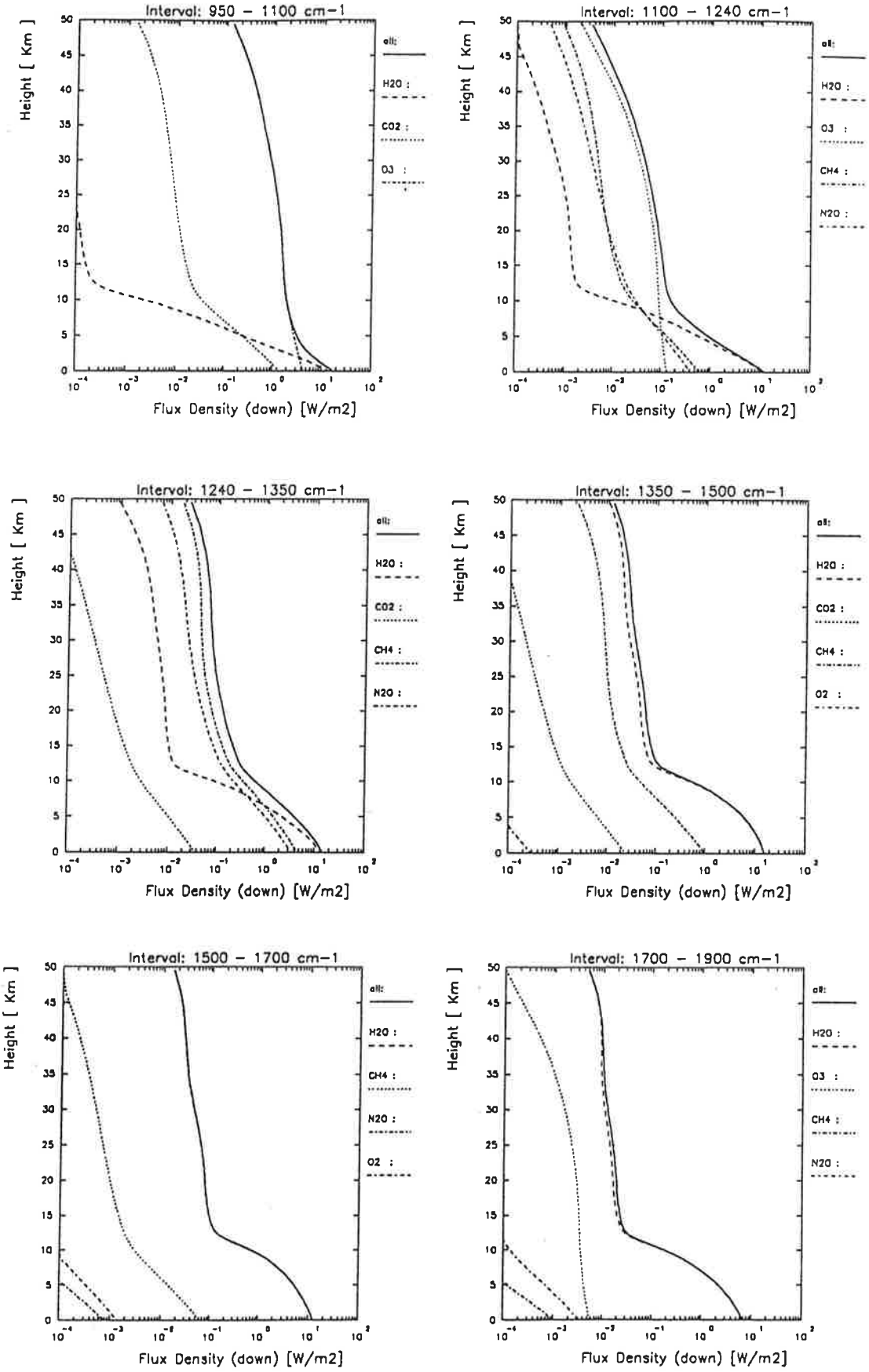

Fig. 10 : continued

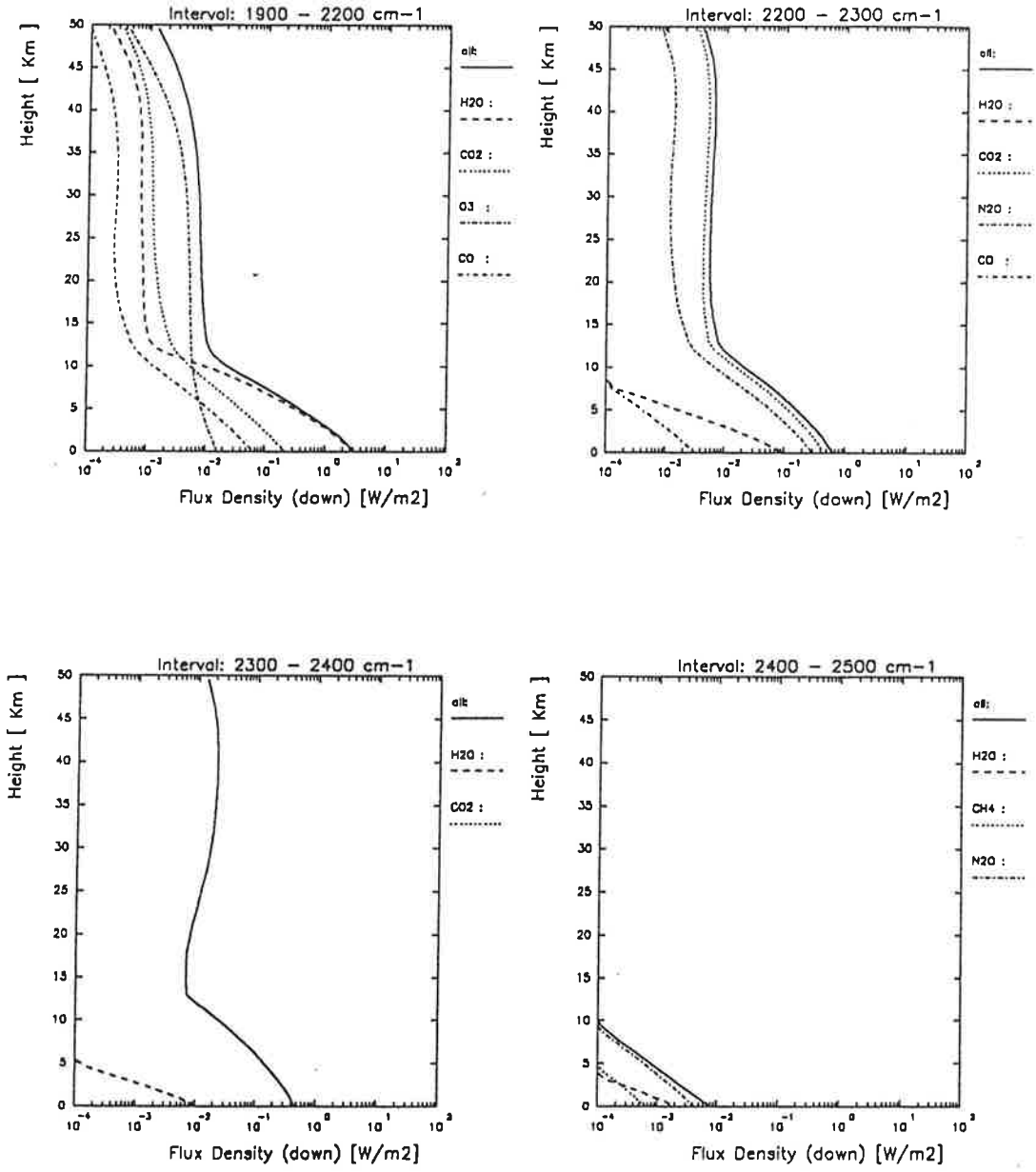

Fig. 10: Downward flux densities in different spectral intervals with the division of the IR according to Fig. 9. The solid curve denotes the contribution of the seven main absorbers.

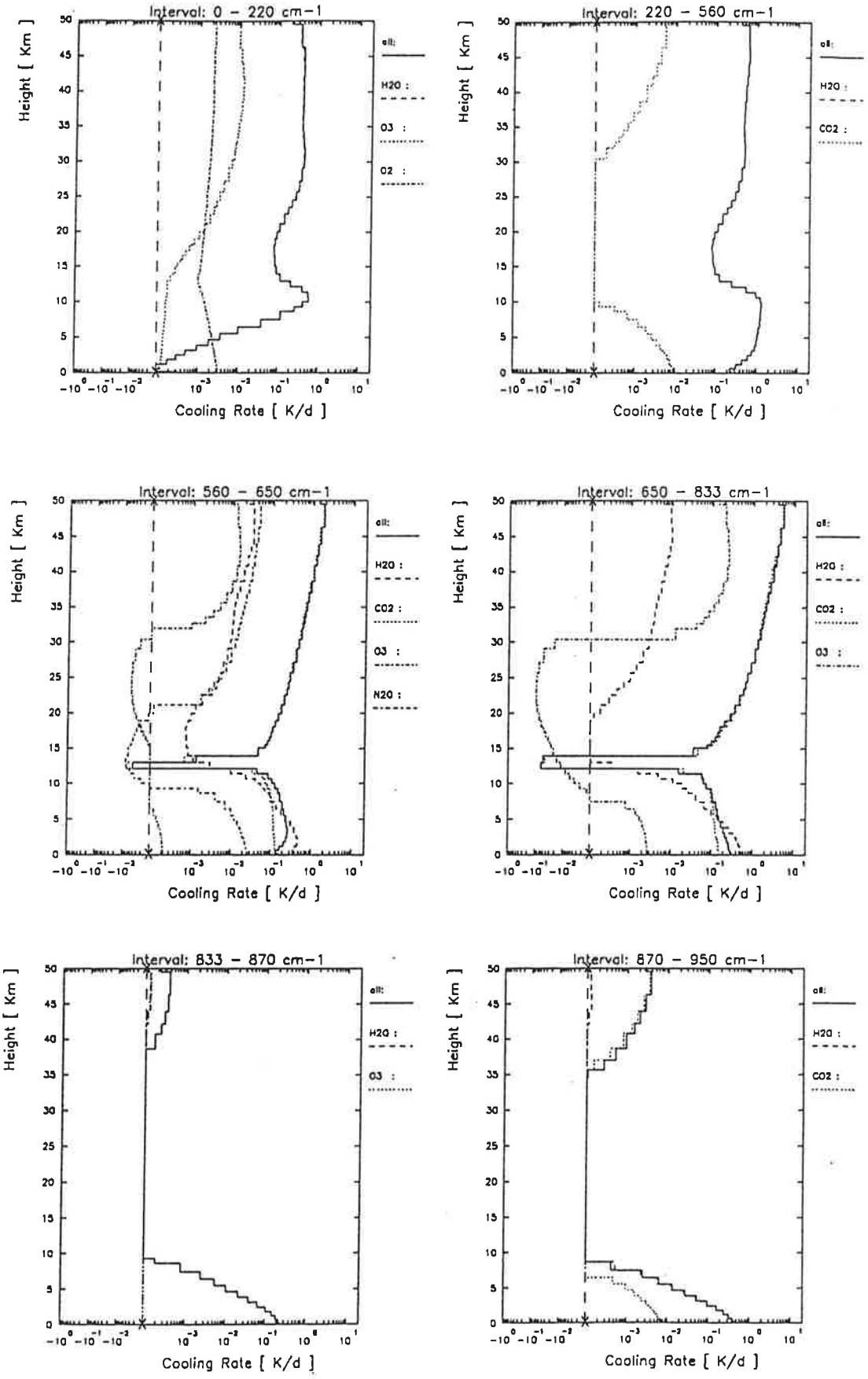

Fig. 11 : continued

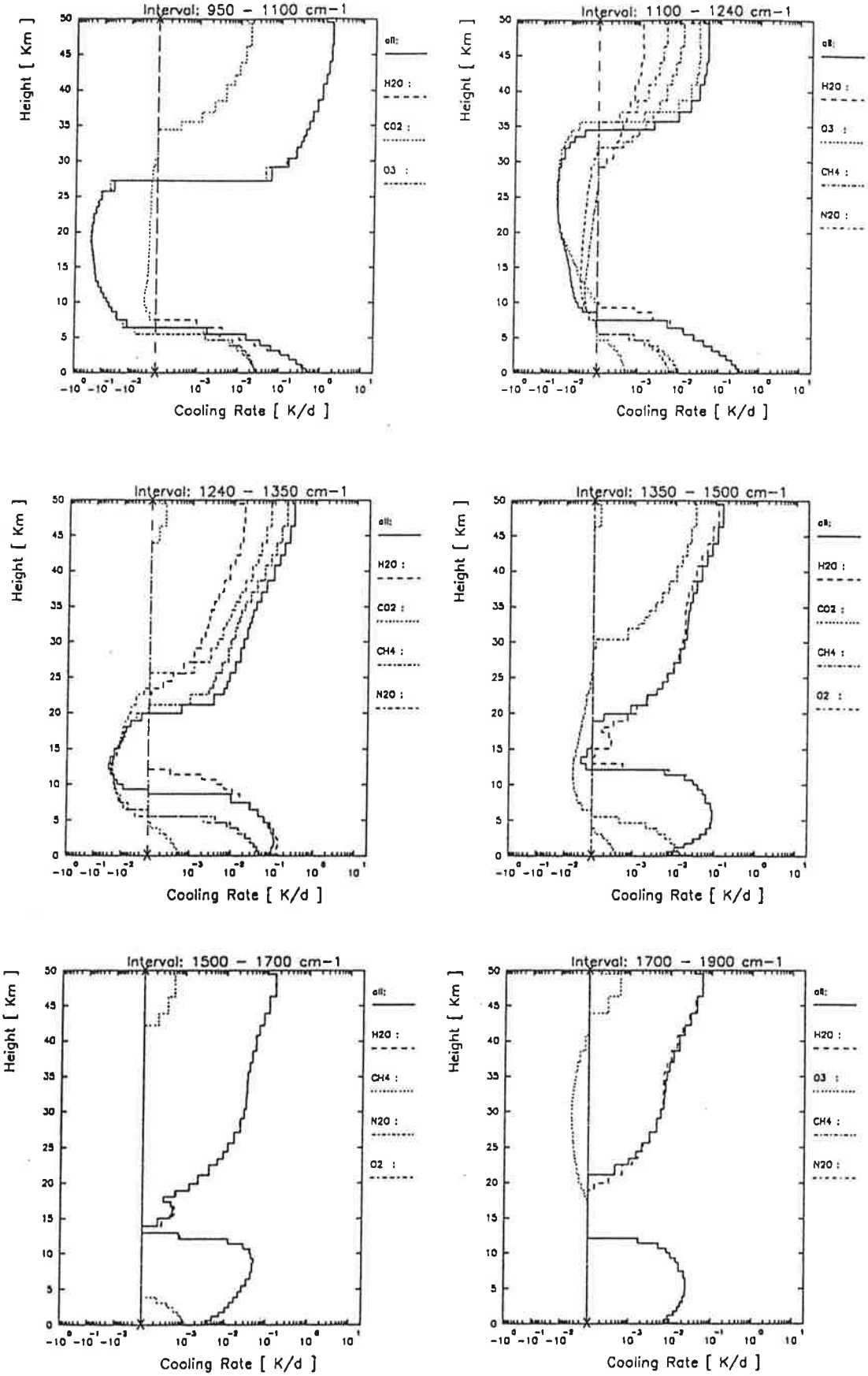

Fig. 11 : continued

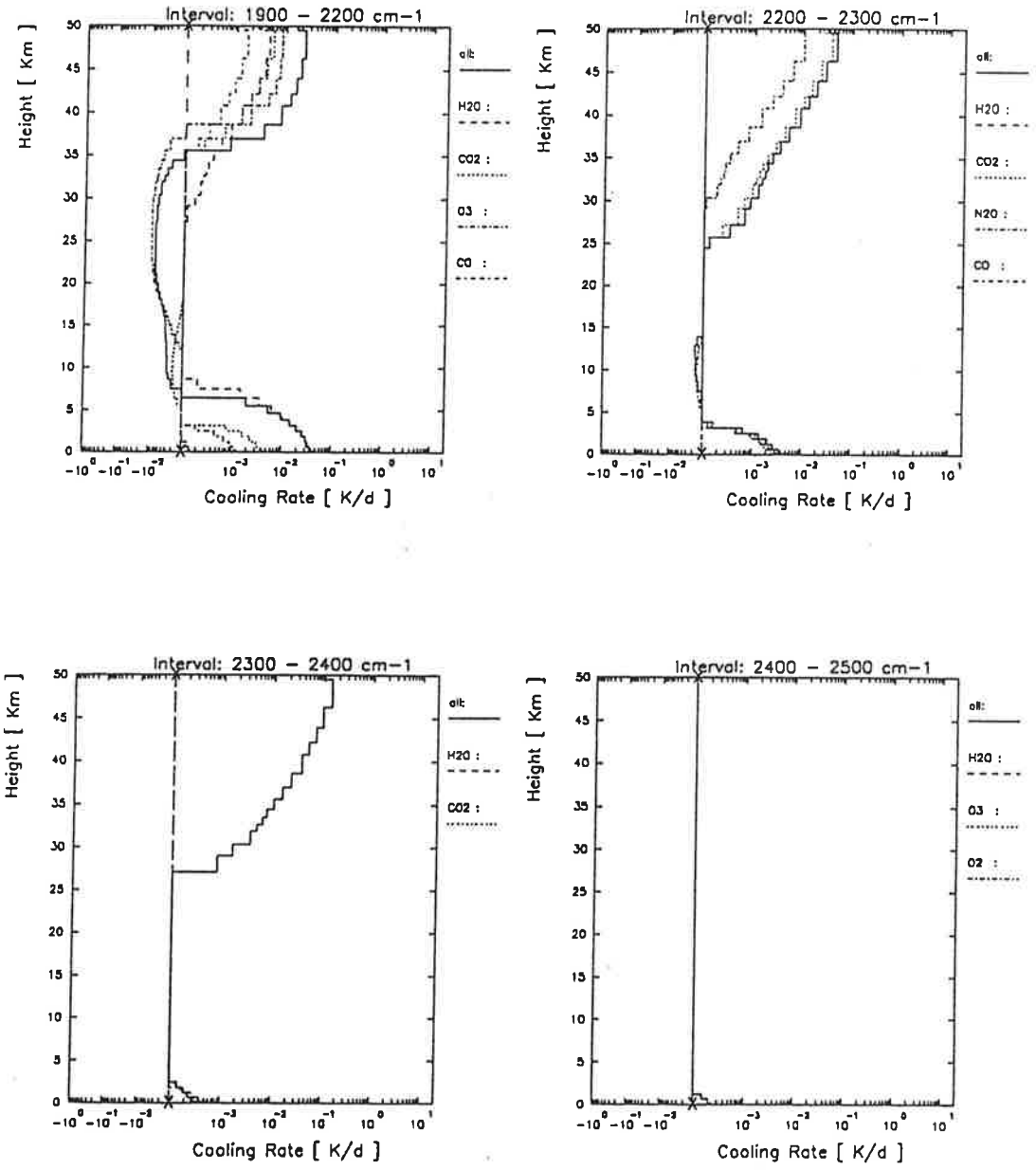

Fig. 11: Atmospheric cooling rates in different spectral intervals with the division of the IR according to Fig. 9. The solid curve denotes the contribution of the seven main absorbers.

With regard to radiation fluxes and cooling rates approximated by narrow or broad band models it is desirable to avoid band overlapping as much as it is reasonabel. Therefore, from the preceding results, the spectral intervals and absorbers are set according to Fig. 12 in order to test whether reliable fluxes and cooling rates can be achieved.

Fig. 12: Division of the IR according to the distribution of absorption bands with neglected weak bands.

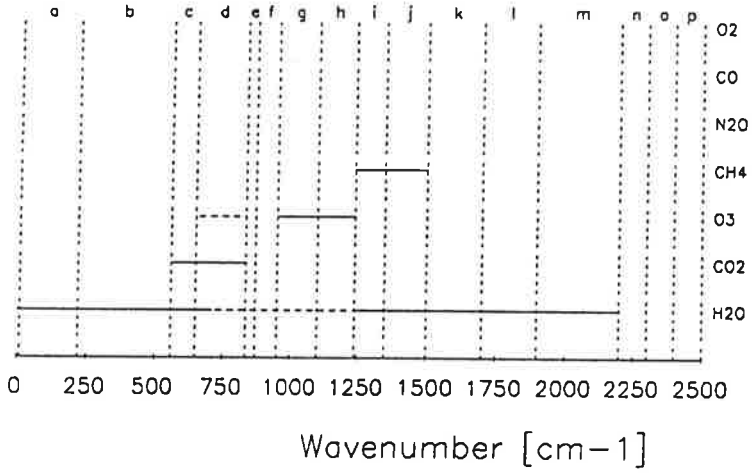

Here the contributions of O_2 , CO , and N_2O to absorption of radiation in the IR are totally neglected, and no absorption at all is considered in the range between 2200 - 2500 cm^{-1}. The comparison of the cooling rates and total flux densities with those obtained with the full consideration of all lines in all parts of the IR is shown in Fig. 13 and 14 (solid curves) in the form of relative and absolute deviations, respectively. The dashed curves result from calculations with additional inclusion of the ozone band at 14 μm (indicated by the dashed line in Fig. 12).

Within the stratosphere cooling rates show deviations up to $\pm$ 10 %. In the region of the tropopause the relative deviations go up to 50 % . However, these large relative deviations only occur where the absolute deviations are small. In the troposphere (below 10 Km) the absolute and relative deviations are small.

The deviations of the upward flux densities (Fig. 14, top) do not exceed 1 % or 3 W/m^2, respectively. For the downward flux densities (Fig. 14, bottom) the

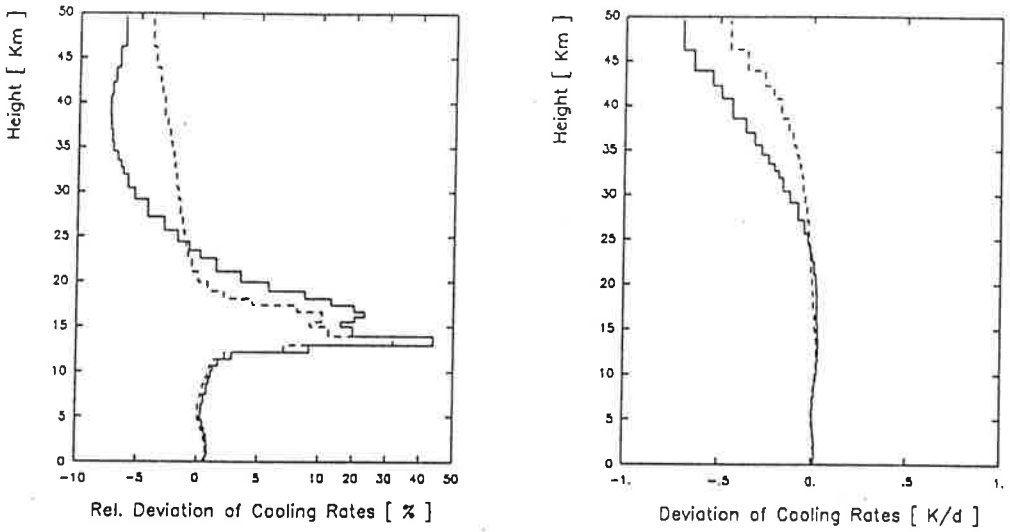

Fig. 13: Deviations of cooling rates of bands corresponding to Fig. 12 from cooling rates with the application of all lines in the IR. Dashed curve with the inclusion of the 14 μm band of ozone.

relative deviations have a maximum of 7 % ($\approx 0.5 W/m^2$) at about 27 Km and get less towards the ground. The absolute deviations, however, increase with decreasing height and reach a maximum of about 2.8 W/m^2 in the lower troposphere. But the inclusion of the 14 μm band of ozone improves the results especially in the lower stratosphere.

However, if weak bands are neglected, the effect of possible or potential changes in the concentration of atmospheric absorbers has to be discussed.

As it can be seen from Fig. 10 for the midlatitude summer atmosphere, the downward flux density in the interval 950 – 1100 cm^{-1} is dominated by ozone in the stratosphere and by water vapor and ozone in the troposphere. The contribution of CO_2 may be neglected concerning the application of narrow and broadband models, which means in the considered interval an error of about 0.7 W/m^2 at the surface.

But, if for example the atmospheric composition is changed by doubling the CO_2 concentration, and by reducing the ozone density to the half and the one for water vapor to the tenth at all levels, then the neglecting of the CO_2 contribution to

downward flux density leads to an error of about 2 W/m^2 at the surface. Therefore, the weak band of CO_2 has to be taken into account.

Nevertheless, neglecting of weak bands in some intervals gives sufficiently accurate fluxes and cooling for any reasonable atmospheric composition.

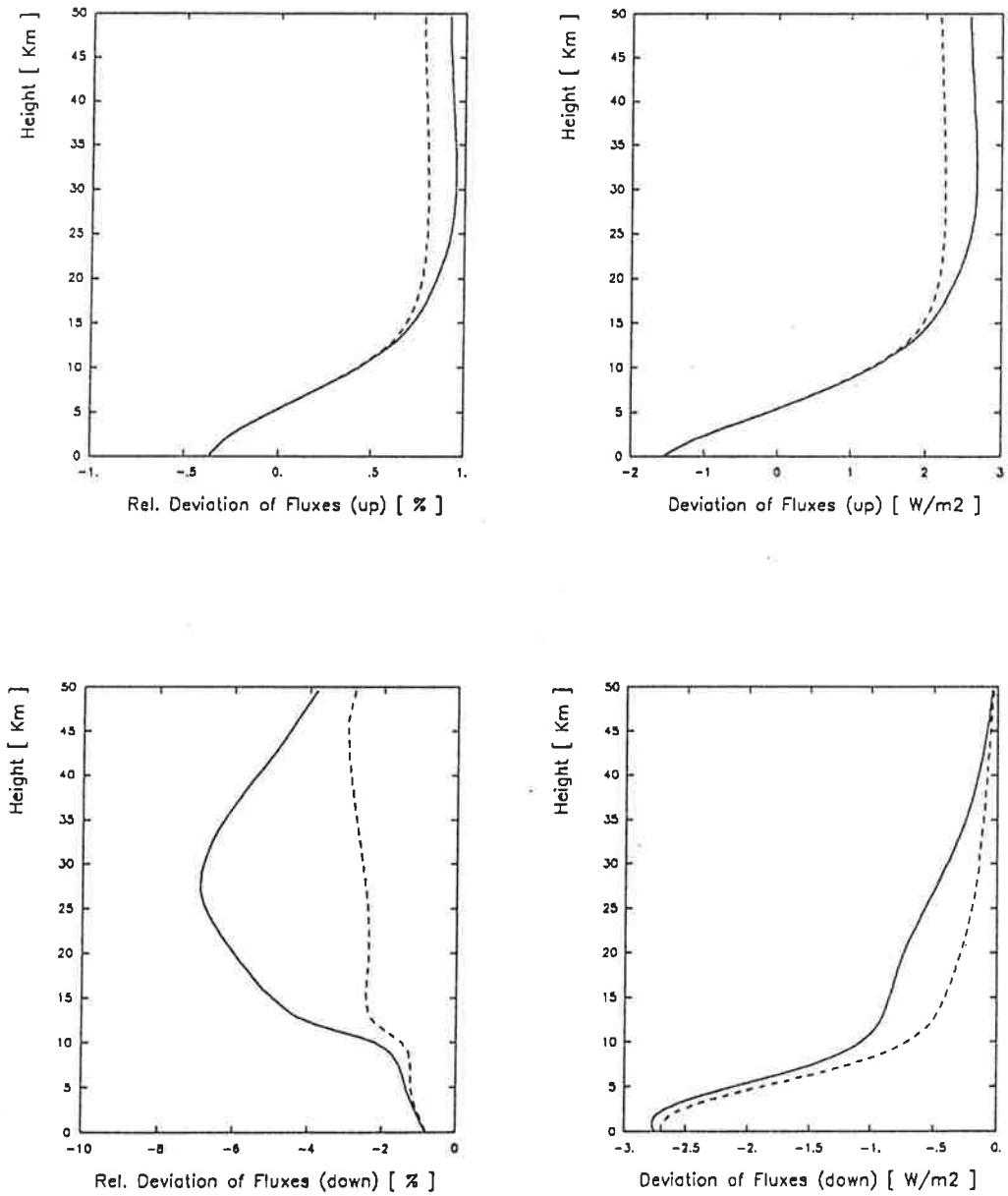

Fig. 14: Deviations of flux densities of bands corresponding to Fig. 12 from flux densities with the application of all lines in the IR. Dashed curve with the inclusion of the 14 μm band of ozone.

5.3
Dependences of Fluxes and Cooling Rates on Error Bounds of the Line Parameters

In using the HITRAN line parameters we assumed in the preceding text that the tabled parameter values are correct. However, these values are not known precisely, because they were obtained by measurments or approximations. Rothman et al. (1986) discuss the error bounds of the line strengths and the halfwidths in detail. In the following a sensitivity study of line-by-line calculations to possible systematic errors is presented. However, not the uncertainty of each line parameter is applied (which is in fact not given), but from the specifications in the HITRAN atlas an average error of 10 % for both, line strengths and halfwidths may be inferred.

For economical reasons the variation of the line strengths and the halfwidths are combined in such a way that the resulting error in the absorption coefficient gets a maximum. From the Lorentz line shape (Eq. 12) and the Voigt line shape (Eq. 13) it is evident that increasing the line strength increases the absorption coefficient in any spectral range, too. For the Lorentz profile enlarging the halfwidth also causes an increase of the absorption coefficients in the wings. Calculations with the Voigt line shape show only little influence of enlarging the halfwidth on the absorption coefficients in the central range at high wavenumbers and (or) low pressure. At high pressure forming the line shape is dominated by collisional broadening and enlarging the halfwidth diminishes absorption according to the Lorentz profile in the central line range. However, it is known that absorption of radiation at high pressure occurs mainly in the wings of absorption lines. Therefore, the strongest influence on absorptions coefficients occur when either the line strengths and the halfwidths are enlarged simultaneously according to their error bounds or when they are diminished at the same time.

In order to get the resulting error bounds of cooling rates and flux densities, the calculations have been performed for: a) the line strengths and halfwidths of the HITRAN parameter atlas were decreased by 10 %, b) the parameter have been used as they are, and c) they have been increased by 10 % . The deviations of the cases a) from b) and c) from b), respectively, are shown in Fig. 15 for the cooling rates and Fig. 16 for the flux densities. There, the solid curves stand for decreasing the line parameters and the dashed ones for an increase.

Only those levels are considered where the absolute deviations are not negligible. Here, the cooling rates show relative deviations up to $\pm$ 4 % in the troposphere

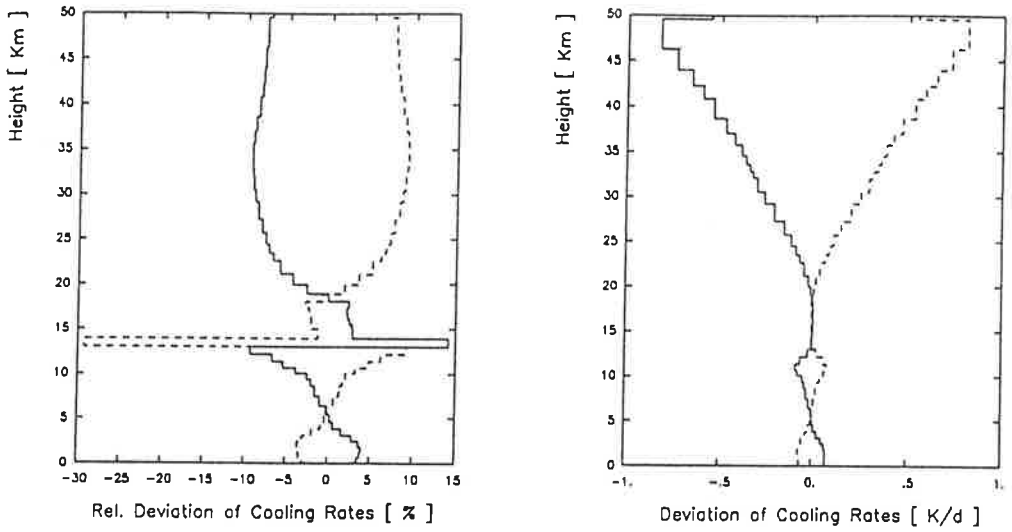

Fig. 15: Deviations of cooling rates from calculated cooling rates with the line parameters assumed to be exact. The assumption of decreasing the line strengths and the halfwidths by - 10 % leads to the solid curve. The dashed curve is due to an increase of 10 % for both.

and up to ± 10 % in the middle stratosphere. The maximum absolute deviation of about ± 0.8 K/d is found in the upper stratosphere.

The upward flux is affected most in the whole troposphere with the consequence that flux densities at the top of the atmosphere show deviations about ± 1.5 % which means about ± 3 W/m^2. The maximum uncertainty for the downward flux densities is even larger. Here we find at the height of 3 Km the amount of about 5 W/m^2.

These mentioned deviations give an idea of the possible uncertainty even of line-by-line flux and cooling rate calculations due to the presently knowledge of line parameter values.

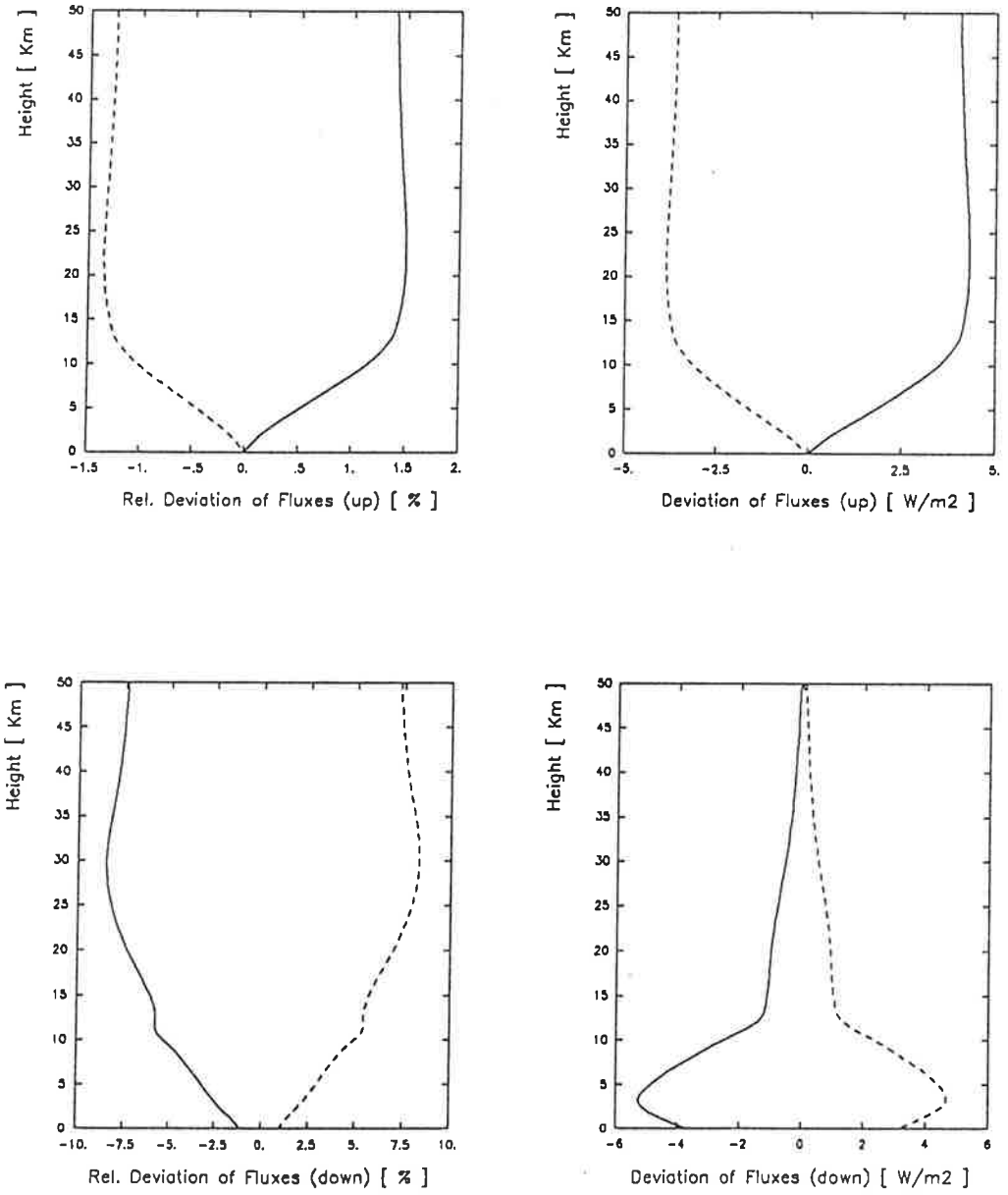

Fig. 16: Deviations of flux densities from calculated flux densities with the line parameters assumed to be exact. The assumption of decreasing the line strengths and the halfwidths by - 10 % leads to the solid curve. The dashed curve is due to an increase of 10 % for both.

6
Summary

In the preceding text a line-by-line model is described which is designed for the purpose of proving the influence of uncertainties of the line shapes and the pressure-temperature dependence of halfwidths as well as affections of numerical properties (orders of numerical quadratures and the subdivision of the IR) on the calculation of radiation fluxes and atmospheric cooling rates.

We have found that in general for large spectral ranges the resolution with constant subintervals of 0.01 cm^{-1} widths in conjunction with an eight point Gaussian quadrature gives high accuracy in the troposphere. For most parts of the stratosphere relative deviations of the cooling rates are less than 0.25 %. In the lower stratosphere the absolute deviations of cooling rates are small so relative deviations up to a few per cent do not matter.

For smaller spectral intervals the division into subintervals of 0.01 cm^{-1} widths gives accurate results for the troposphere, too. But for the stratosphere this may lead to deviations of several per cent for the cooling rates in spectral ranges with a large number of isolated lines. Here the application of the DLD resolution scheme is advantageous which agrees well with the resolution by subintervals of the constant widths 0.001 cm^{-1} (the latter needs more computation time).

To estimate the influence of overlapping bands the IR is divided into 16 subintervals and calculations of fluxes and cooling rates were carried out for each of these. There, we have considered each of the seven main absorbers seperately and the effect of overlapping of all lines of all absorbers. It has been found that for those applications, where a 10 % accuracy of cooling rates would be sufficient, it is possible to use the mentioned intervals with the consideration of only two absorption bands in each. However, for the range 650 – 800 cm^{-1} the additional inclusion of the 14 μm ozone band to the bands of H_2O and CO_2 improves the results in the stratosphere. It is also necessary to include the 10.4 μm CO_2 band additionally to the 9.6 μm ozone band and the water vapor continuum range, if drastically enlarged carbon dioxide concentrations are considered.

Finally, we have tried to estimate an uncertainty range for cooling rates and fluxes due to errors in the line parameters by the rough assumption that all line strengths and halfwidths are uncertain by about $\pm$ 10 %. A more detailed consideration of the uncertainties of the individual line parameters would probably

narrow the error margin, because the strengths of strong lines are better known than those of weak. On the other hand effects of the badly known dependence of the halfwidths on temperature have not been considered. This is also true for uncertainties of absorption line shapes. However, a further examination of this and considerations concerning the integration of the equation of the optical thickness, notably for larger atmospheric layers, would be certainly more economic by approximation algorithms if these are available for calculations of fluxes and cooling rates with sufficient accuracy.

References

Armstrong, B.H., 1967. Spectrum Line Profiles: The Voigt Function. J. Quant. Spectrosc. Radiat. Transfer, 7, 61 - 88.

Burch, D.E., D.A. Gryvnak, R.R. Patty, and C.E. Bartky, 1969. Absorption of Infrared Radiant Energy by CO_2 and H_2O. IV. Shapes of Collision--Broadened CO_2 Lines. J. Opt. Soc. Am., 59, 267 - 280.

Burch, D.E. and D.A. Gryvnak, 1980. Continuum Absorption by H_2O Vapor in the Infrared and Millimeter Regions. From "Atmospheric Water Vapor", ed. by Deepak, A., T.D. Wilkerson, and L. H. Ruhnke. Academic Press Inc., London.

Chesters,D. and A. Arking, 1985. Cited in Chou and Kouvaris (1986) as private communication

Chou, M.-D. and A. Arking, 1980. Computation of Infrared Cooling Rates in the Water Vapor Bands. J. Atmos. Sci., 37, 855 - 867.

Chou. M.-D. and L. Kouvaris, 1986. Monochromatic Calculations of Atmospheric Radiative Transfer due to Molecular Line Absorption. J. Geophys. Res., 91, 4047 - 4055.

Drayson, S. R., 1966. Atmospheric Transmission in the CO_2 Bands between 12 μ and 18 μ. Appl. Opt., 5, 385 - 391.

Drayson, S. R., 1976. Rapid Computation of the Voigt Profile. J. Quant. Spectrosc. Radiat. Transfer, 16, 611 - 614.

Fels, S. B. and M. D. Schwarzkopf, 1981. An Efficient, Accurate Algorithm for Calculating CO_2 15 μm Band Cooling Rates. J. Geophys. Res., 86, 1205 - 1232.

Goody, R. M., 1964. Atmospheric Radiation, Theoretical Basis. Oxford at the Clarendon Press.

Herbert, F., 1974. Spectrum Line Profiles: A Generalized Voigt Function Including Collisional Narrowing. J. Quant. Spectros. Radiat. Transfer, 14, 943 - 951.

Herzberg, G., 1945. Infrared and Raman Spectra.
Van Nostrand Reinhold Company, New York.

Kunde, V. G. and W. C. Maguire, 1974. Direct Integration Transmittance Model.
J. Quant. Spectrosc. Radiat. Transfer, 14, 803 - 817.

Liou, K.-N., 1980. An Introduction to Atmospheric Radiation. International
Geophysics Series, Vol. 26., Academic Press Inc., London.

Liu, Q. and J. Schmetz, 1988. On the Problem of an Analytical Solution to the
Diffusivity Factor. Beitr. Phys. Atmosph. 61, 23 - 29.

Matveyev V.S., 1972. Approximate Representations of the Absorption Coefficient
and Equivalent Width with the Voigt Shape. J. Appl. Spectros.(USSR), 16, 228 - 233.

McClatchey, R. A., R. W. Fenn, J.E.A. Selby, F. E. Volz, and J. S. Garing, 1978.
Optical Properties of the Atmosphere.
Handbook of Optics, McGraw-Hill, sec. 14, pp 14-1 - 14-65.

Morcrette, J.-J. and Y. Fouquart, 1985. On Systematic Errors in Parametrized
Calculations of Longwave Radiation Transfer.
Quart. J. R. Met. Soc., 111, 691-708.

Pierluissi, J. H., P. C. Vanderwood, and R. B. Gomez, 1977. Fast Calculational
Algorithm for the Voigt Profile.
J. Quant. Spectrosc. Radiat. Transfer, 18, 555 - 558.

Poesener, D. W., 1959. The Shape of Spectral Lines: Tables of the Voigt Profile.
Aust. J. Phys., 12, 184 - 196.

Roberts, R. E., J. E. Selby, and L. M. Biberman, 1976. Infrared Continuum
Absorption by Atmospheric Water Vapor in the 8-12-μm Window.
Appl. Opt., 15, 2085 - 2090.

Rodgers, C. D., 1976. Collisional Narrowing: Its Effect on the Equivalent Widths
of Spectral Lines. Appl. Opt., 15, 714 - 716.

Rothman, L. S., 1981. AFGL Atmospheric Absorption Line Parameters Compilation:
1980 Version. Appl. Opt., 20, 791 - 795.

Rothman, L. S., R. R. Gamache, A. Goldman, L. R. Brown, R. A. Toth, H. M. Pickett,
R. l. Poynter, J.-M. Flaud, C. Camet-Peyret, A. Barbe, N. Husson, C. P. Rinsland,
and M. A. H. Smith, 1987. The HITRAN Database: 1986 Edition.
Appl. Opt. 26, 4058 - 4097.

Scott, N. A., 1974. A Direct Method of Computation of the Transmission Function
of an Inhomogeneous Gaseous Medium - I: Description of the Method.
J. Quant. Spectrosc. Radiat. Transfer, 14, 691 - 704.

Scott, N. A. and A. Chedin , 1981. A Fast Line-by-Line Method for Atmospheric Computations: The Automatized Atmospheric Absorption Atlas. J. Appl. Meteor., 20, 802 - 812.

Stephens, G. L., 1984. The Parameterization of Radiation for Numerical Weather Prediction and Climate Models. Mon. Wea. Rev., 112, 826 - 867.

Whiting, E. E., 1968. An Empirical Approximation to the Voigt Profile. J. Quant. Spectrosc. Radiat. Transfer, 8, 1379 - 1384.

World Meteorological Organization, 1984. The Intercomparison of Radiation Codes in Climate Models (ICRCCM), Longwave Clear Sky Calculations. Report of a meeting in Frascati, Italy, 15-18 August 1984, World Climate Programme Report WCP-93, available from WMO, Geneva, Switzerland, 37.

Zdunkowski, W. G., G. J. Korb, and C. T. Davis, 1974. Radiative Transfer in Model Clouds of Variable and Height Constant Liquid Water Content as Computed by Approximate and Exact Methods. Contr. Atmos. Phys., 47, 157 - 186.